nature communications

Article

https://doi.org/10.1038/s41467-025-61664-7

Northern peatland microbial communities exhibit resistance to warming and acquire electron acceptors from soil organic matter

Received: 17 July 2024

Accepted: 25 June 2025

Published online: 25 July 2025

Check for updates

Katherine Duchesneau[1,10], Borja Aldeguer-Riquelme[2,10], Caitlin Petro[1], Ghiwa Makke[3], Madison Green[1], Malak Tfaily[3], Rachel Wilson[4], Spencer W. Roth[5], Eric R. Johnston[6], Laurel A. Kluber[6], Christopher W. Schadt[6], Jesse B. Trejo[7], Stephen J. Callister[7], Samuel O. Purvine[8], Jeffrey P. Chanton[4], Paul J. Hanson[6], Susannah Tringe[9], Emiley Eloe-Fadrosh[9], Tijana Glavina del Rio[9], Konstantinos T. Konstantinidis[2] & Joel E. Kostka[1] ✉

The response of microbial communities that regulate belowground carbon turnover to climate change drivers in peatlands is poorly understood. Here, we leverage a whole ecosystem warming experiment to elucidate the key processes of terminal carbon decomposition and community responses to temperature rise. Our dataset of 697 metagenome-assembled genomes (MAGs) represents the microbial community from the surface (10 cm) to 2 m deep into the peat column, with only 3.7% of genomes overlapping with other well-studied peatlands. Community composition has yet to show a significant response to warming after 3 years, suggesting that metabolically diverse soil microbial communities are resistant to climate change. Surprisingly, abundant and active methanogens in the genus *Candidatus* Methanoflorens, *Methanobacterium*, and *Methanoregula* show the potential for both acetoclastic and hydrogenotrophic methanogenesis. Nonetheless, the predominant pathways for anaerobic carbon decomposition include sulfate/sulfite reduction, denitrification, and acetogenesis, rather than methanogenesis based on gene abundances. Multi-omics data suggest that organic matter cleavage provides terminal electron acceptors, which together with methanogen metabolic flexibility, may explain peat microbiome composition resistance to warming.

Northern peatlands, which are often dominated by peat mosses (*Sphagnum* spp.[1]) and characterized by their waterlogged organic soils[2], contain approximately half of Earth's soil carbon[3]. The peatland "carbon bank" is a consequence of the intricate balance between plant productivity and slow decomposition rates of soil organic matter (SOM). *Sphagnum* spp. mosses are thought to play a key role in carbon sequestration. They act as ecosystem engineers, fostering acidic, nitrogen- and phosphate-poor conditions, and retaining water to create anaerobic environments that impede SOM decomposition[4–6]. Northern peatlands face mounting threats, with more pronounced warming projected at high latitudes in comparison to global averages[7–10]. The heterotrophic microbial communities that mediate SOM decomposition and the release of greenhouse gases (carbon dioxide, CO_2; methane, CH_4) are expected to be stimulated by warming[11–15]. However, our ability to predict the rates and controls of SOM decomposition in peatland soils is hindered by a limited understanding of the microbial communities involved.

A full list of affiliations appears at the end of the paper. ✉e-mail: joel.kostka@biology.gatech.edu

Peatland soils differ profoundly in physical, chemical, and biological characteristics compared to their better understood upland forest counterparts. Upland forest soils are generally not saturated with water and oxygen is more available for microbial utilization. Thus, most SOM degradation is thought to occur under aerobic conditions and decomposition is hypothesized to be limited by carbon substrate availability[16,17]. In contrast, water-saturated soils of *Sphagnum*-dominated peatlands are defined by anoxia, a paucity of inorganic terminal electron acceptors (TEAs), and respiratory pathways that mediate the terminal decomposition of organic matter are likely rate limiting[18–21]. Carbon fixed by live vegetation is rapidly oxidized to CO_2 above the water table, where oxygen is available[11,12,19]. Immediately below the water table, fermentation products often accumulate in peat porewaters in temperate and high latitude peatlands[11,19], indicating that terminal electron accepting processes (TEAPs) become rate limiting in the absence of oxygen. In this zone, SOM degradation is mediated by mainly anaerobic processes[12,22]. Anaerobic laboratory incubation experiments corroborate field observations, showing that amendments of peat with energetically favorable, non-fermentable electron donors such as acetate and formate do not enhance mineralization, as evidenced by minimal changes in greenhouse gas production rates[23]. Conversely, a substantial increase in CO_2 production is observed immediately after the introduction of nitrate[23] and sulfate[24], highlighting the limitation imposed on respiration by TEAs[23,25–27]. Further, and despite TEA limitation under anaerobic conditions, several studies in temperate peatlands have consistently reported 10 to 1000 times higher CO_2 production relative to CH_4[11,23,28–32]. Since the stoichiometry of methanogenesis predicts a 1:1 ratio of CO_2 to CH_4 production, higher ratios of CO_2:CH_4 implicate the predominance of alternative TEAPs[33,34]. Fermentation products that accumulate at in situ temperatures are consumed at elevated temperatures and increase CO_2 production, providing evidence that warming somewhat alleviates the limitation of terminal decomposition[23,35]. This finding suggests that TEAs might be released from the degradation of organic matter itself, a hypothesis that remains to be tested.

A growing body of research has employed metagenomic approaches to uncover the community dynamics and metabolic potential of microorganisms in peat soils[36–41]. The focus has been on the initial steps in SOM degradation (carbohydrate-active enzymes) in acidic, carbon-rich peats dominated by *Sphagnum* spp., where members of the *Acidobacteriota* as well as microbial groups that mediate methane cycling were shown to dominate the soil microbial communities[12,41]. Genes encoding diverse hydrolases believed to be specific for *Sphagnum*-derived carbon compounds were uncovered and the genomic potential for respiration of fermentation products (acetate) was linked to the *Acidobacteriota* at the oxic–anoxic interface[36]. Extensive investigations at Stordalen Mire, a Swedish peatland containing a permafrost thaw gradient, led to the recovery of over a thousand metagenome-assembled genomes (MAGs) and the identification of *Methanoflorens* as a keystone group of methanogens in peatlands[41–44]. However, less attention has focused on terminal decomposition processes other than methanogenesis.

The Spruce and Peatland Responses Under Changing Environments (SPRUCE) experiment, combines air and peat warming in a whole-ecosystem manipulation experiment which aims to understand the impact of climate change drivers (warming and elevated atmospheric CO_2) on ecosystem functioning in a forested peat bog in northern Minnesota. During the first three years of the SPRUCE experiment, warming led to significant increases in greenhouse gas production[45], and surface peat layers became more methanogenic as CH_4 production rates increased more than CO_2 production rates[12]. Preliminary metagenomic analysis suggested that, despite the increase in CH_4 production, the abundance of methanogens remained stable[12]. Notwithstanding these recent insights, the influence of warming on other functional guilds, such as sulfate reducers or acetogens, has not yet been addressed, leaving a critical gap in our understanding of the effects of temperature on peat-dwelling microorganisms. In addition, the metabolic networks that drive the terminal steps of carbon turnover remain to be elucidated, hindering our ability to predict their response to climate change.

This study provides an extensive genome characterization of the microorganisms living in peatland systems for a North American site. Here, we establish a framework to understand how organic matter is processed in soils of this anaerobic, oligotrophic, carbon-rich ecosystem by examining the metabolic potential and microbe-metabolite interactions along a 2 m depth gradient. Furthermore, we leverage this framework in combination with the SPRUCE experiment to begin elucidating how the community of microorganisms mediating organic matter degradation in northern peat soils can be resistant[46] to warming. Our results underscore that the wide metabolic versatility of abundant species may allow them to adapt their activity without significantly changing their abundance. The uncovered taxonomic and metabolic novelty of microbes along with our proposed conceptual model alter perceptions of anaerobic respiration pathways mediating terminal decomposition in peatlands and provide a mechanistic framework for improved predictions of the ratio of CO_2:CH_4 emissions.

Results and Discussion

SPRUCE peat harbors a plethora of undescribed taxa structured by depth

We sequenced 2.4 terabasepairs (Tbp) of metagenomic sequence data from 131 samples collected in 2015, 2016, and 2018 (5–40 Gbp of quality-processed data per sample), which are supported by biogeochemical and metabolomic data collected in parallel (Supplementary Information for a detailed description of the metabolic data). Metagenome binning resulted in the recovery of 697 medium- to high-quality MAGs (more than 50% complete and less than 10% contaminated, Data S1) dereplicated at the species level (i.e., average nucleotide identity [ANI] >95%). The MAG dataset well represents overall microbial richness at the site as evidenced by recruitment of the total metagenomic reads that could be mapped with representative MAGs. The lowest average read recruitment was observed at the peat surface 10–20 cm layer (28.7% of total reads) whereas at the three deeper depth intervals (40–50, 100–125, and 150–175 cm) on average 65, 67.4, and 67.7% of total reads were represented in the MAG dataset, respectively (Figure S1). Depth was the main driver of variation in microbial community composition ($P = 0.002$, $adjR^2 = 0.13$, Fig. 1A, B) and functional potential ($P < 0.001$, $R^2 = 0.623$). Taxonomically, SPRUCE MAGs belong to a diverse range of bacterial (620 genomes) and archaeal phyla (77 genomes). Specifically, we recovered MAGs from 33 phyla (Fig. 1B, C), including *Bacteria* belonging to *Acidobacteriota* (222 MAGs), *Actinomycetota* (75), *Proteobacteria* (64) and *Verrucomicrobiota* (48), and Archaea from the *Thermoproteota* (45) and *Halobacteriota* (17). Genomes of diverse aerobic chemoorganoheterotrophs were abundant in surface peat, while the deeper depths were predominated by taxa known for their anaerobic metabolism. *Acidobacteriota* was the most abundant phylum at all depths, with the highest abundance observed in surface peat (10–20 cm). Similarly, *Actinomycetota* and *Pseudomonadota* were more abundant in the surface layer. At mid depth (40–50 cm) we found a peak in the relative abundance of Desulfobacterota_B and *Halobacteriota* while the deep peat (100–125 and 150–175 cm) was the preferred habitat for *Thermoproteota*, *Thermoplasmatota*, *Verrucomicrobiota* and *Chloroflexota* (Fig. 1B). This taxonomic stratification is a consequence of the metabolic distribution across the vertical profile in response to TEA availability and organic matter quality, as we show below.

The SPRUCE MAGs represent undescribed taxa, with the large majority (79.5%) belonging to genera that have not been formally

https://doi.org/10.1038/s41467-025-61664-7

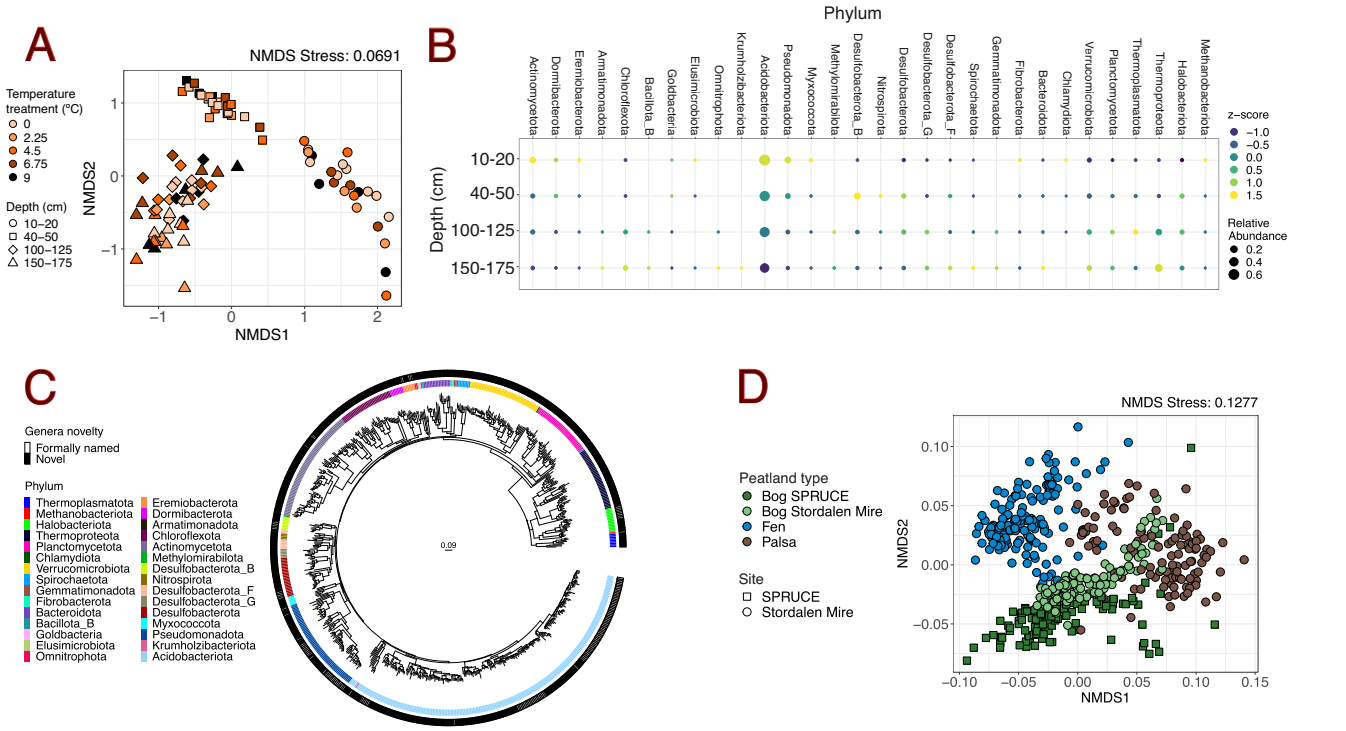

Fig. 1 | Depth distribution and taxonomic novelty of the metagenome-assembled genomes (MAGs) recovered from SPRUCE peat. A Non-metric Multi-Dimensional Scaling (NMDS) plot based on MASH distances of metagenomes collected from SPRUCE in 2016 and 2018. The temperature treatment is indicated with colors while depth is shown with different shapes. **B** Bubble plot showing the taxonomic distribution at the phylum level (x-axis) along the vertical profile (y-axis). Dot size is proportional to the aggregated relative abundance (TAD80/GEQ) of each phylum while color shows the z-score value (the more positive the z-score is, the higher is the preference for that layer). Missing dots indicate the phylum was not detected at that depth. **C** Phylogenomic tree based on 400 universal genes. Inner ring shows the taxonomic classification of each MAG at the phylum level. Outer ring indicates whether the MAG belongs to a formally named genera (white) or remains unnamed (black). Note that the majority lack a formal description. **D** Non-metric Multi-Dimensional Scaling (NMDS) plot based on MASH distances of metagenomes from SPRUCE (squares) and Stordalen Mire (circles). Colors indicate the type of peatland (bog, palsa or fen). Note the clear geographical clustering of the samples.

described following the rules of either the ICNP or SeqCode. Furthermore, 20.8% and 4.6% of all MAGs were from an undescribed order and undescribed class, respectively (Fig. 1C). The novelty of the SPRUCE soil microbiome was also supported by comparison against metagenomes retrieved from a broad range of global soil types (upland forest, tropical, Antarctic, grassland, and managed agricultural ecosystems) (Fig. S2), revealing that SPRUCE peat harbors a plethora of ecosystem-specific, undescribed microbial taxa. To further examine the distinct characteristics of the dataset, we specifically compared our SPRUCE metagenomes against metagenomes from Stordalen Mire, a Swedish peatland with similar features to SPRUCE (type of soil, latitude, temperature, pH) as a well-studied global reference point with detailed, publicly available metagenomic analyses[41,47]. A non-metric multi-dimensional scaling (NMDS) plot based on MASH distances of raw reads revealed clustering by peatland type (bog, fen, palsa, $P = 0.001$, adj$R^2 = 0.31$, Fig. 1D, Fig. S3) and site (SPRUCE vs Stordalen Mire, $P = 0.001$, adj$R^2 = 0.14$, Fig. 1D, Figure S3), further highlighting the novelty of these peat metagenomes with respect to previous work. In addition, only 26 of the total MAGs recovered in the present study (3.7%) shared more than 95% ANI to MAGs reported by Woodcroft, et al.[41] from Stordalen Mire. Most of these shared genomes were members of the phylum *Acidobacteriota* (8 MAGs), *Actinomycetota* (7 MAGs), and *Halobacteriota* (4 MAGs). Of particular interest, 5 out of the 26 MAGs belonged to Candidatus species named by Woodcroft et al.[41]. For example, SPRUCE 382 was assigned to *Ca*. Acidiflorens clade 2, SPRUCE 682 to *Ca*. Acidiflorens stordalenmirensis, SPRUCE 50 to *Ca*. Changshengia, SPRUCE 210 to *Ca*. Methanoflorens crillii, and SPRUCE 510 to *Ca*. Methanoflorens stordalenmirensis, the dominant methanogen genome in Stordalen Mire.

Microbial community composition remains stable in response to warming despite changes in gas fluxes

The MAG composition-based NMDS and db-RDA analyses of samples collected in 2016 and 2018 did not reveal any significant effects of warming or eCO_2 on overall microbial community composition at any of the sampled depths (Fig. 1A). There were no significant changes in the relative abundance of any of the functional groups with temperature at any depth (Fig. 2). Furthermore, the abundance of only a small subset of genomes (6.7%) appeared to correlate with the temperature treatments (Data S2). Broadly the community does not respond to warming, i.e. it is resistant to this disturbance (Allison & Martiny, 2008) despite the sensitivity of CO_2 and CH_4 emission rates with warming[11,12]. This could be explained by the slow generation time of soil bacteria[48], which may not complete a generation in ecosystems with short growing seasons[49].

Biogeochemical data from previous studies at SPRUCE (that is, using the same experimental design) have shown that the ratio of CO_2 to CH_4 in the peat declined with warming at the surface because of increased CH_4 over CO_2 emissions, indicating that the peatland ecosystem is becoming more methanogenic[11,12]. Rate measurements of acetogenesis and methanogenesis conducted in summer of 2018 at SPRUCE, coinciding in space and time with our metagenomic dataset, also showed that rates of homoacetogenesis increased with temperature[50]. Broadly, metabolite composition remained stable along the warming and eCO_2 treatments through the depth profile (Fig. S4). However, more thorough examinations of organic matter molecular composition at SPRUCE have revealed that the aerobic, surface layer of peat is degraded more readily with warming[51,52], possibly due to interactions between plants and their root associated

https://doi.org/10.1038/s41467-025-61664-7

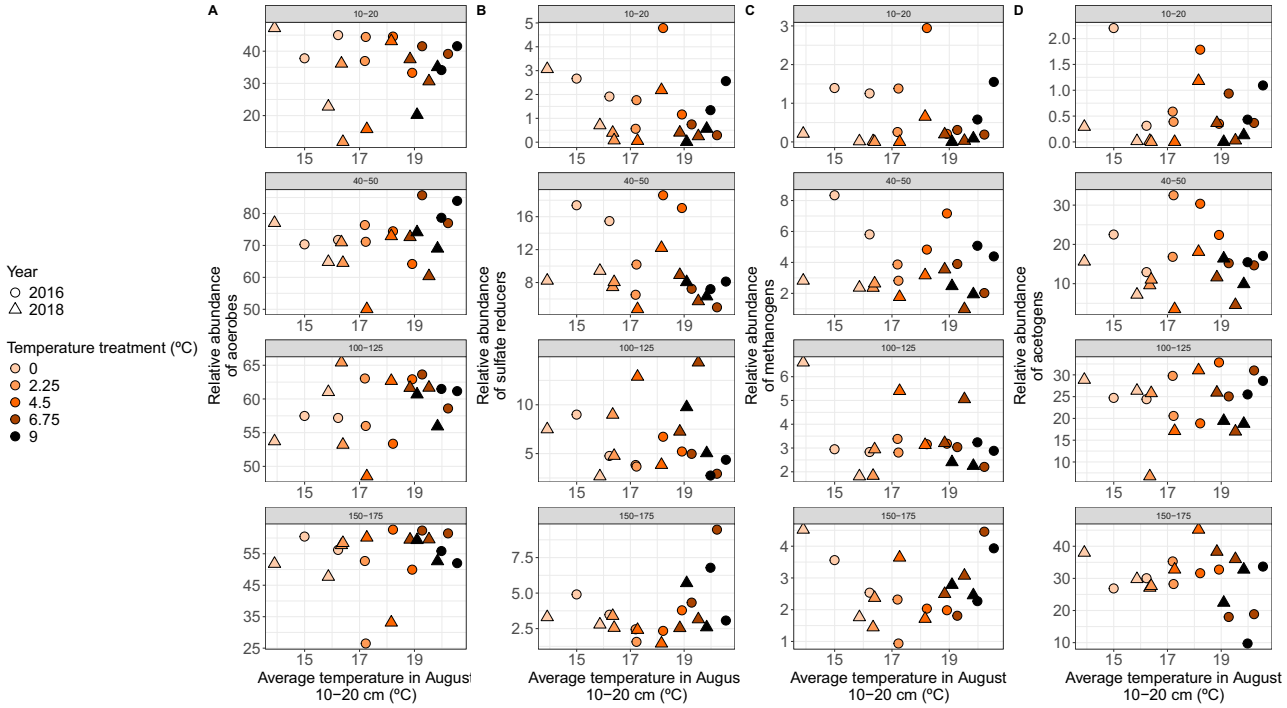

Fig. 2 | Warming treatment does not significantly impact the relative abundance of functional guilds. A Mean aggregated relative abundance (TAD80/GEQ, x-axis) of MAGs encoding for aerobic respiration over the average temperature in August of the same year from 10–20 cm of the surface (°C, y axis). **B** Mean aggregated relative abundance (TAD80/GEQ, x-axis) of MAGs encoding for sulfate reduction over the average temperature in August of the same year from 10–20 cm of the surface (°C, y axis). **C** Mean aggregated relative abundance (TAD80/GEQ, x-axis) of MAGs encoding for methanogenesis over the average temperature in August of the same year from 10–20 cm of the surface (°C, y axis). **D** Mean aggregated relative abundance (TAD80/GEQ, x-axis) of MAGs encoding for the Wood-Ljundahl pathway of acetogenesis over the average temperature in August of the same year from 10–20 cm of the surface (°C, y axis). Color indicates warming treatment, and shape indicates year when samples were collected. Each row represents a distinct depth interval from 10 to 175 cm below the peat surface.

microbes[53]. Thus, the response of peat microbes to warming at the community level must be (if any) smaller than the response in their activity. To identify potential mechanisms underlying the discrepancy between stable microbial community composition and increased gas emissions under warming, we explored the potential metabolic capabilities of peat microbes and developed a conceptual model. This model illustrates the main microbial metabolic mechanisms driving carbon decomposition and CH_4 and CO_2 emissions across the peat vertical profile.

Previously undescribed and abundant peat genomes reveal a broad metabolic diversity

We first focus on the most abundant MAGs, which exhibited a versatile metabolic potential, with the ability to perform two or more of the energy-generating pathways described above (Fig. S5). Metabolic potential was confirmed when at least half of the genes in the KEGG pathway, along with key genes (e.g., *fdh* for the Wood–Ljungdahl pathway), were annotated in the MAG. We present a few metabolic models before delving into our conceptual model to illustrate this metabolic flexibility.

A small but growing body of evidence reveals that members of the *Acidobacteriota*, a ubiquitous soil lineage, are capable of sulfate respiration in peat soils[54]. Recent work based on lab incubations confirmed and extended these observations, showing the potential for both aerobic respiration and sulfate reduction in the same *Acidobacteriota* genome[55]. *Acidobacteriota* MAGs in our dataset further corroborate these findings. For example, SPRUCE 682, with an average 3.2% relative abundance at the 40-50 cm, shows the potential to respire oxygen and/or sulfate. This genome, which belongs to the genus *Ca*. Acidiflorens (Sba1), also shows the potential to obtain sulfate by cleaving organic-sulfur compounds, such as choline-O-sulfate (Fig. 3). SPRUCE 586 is another interesting genome within the *Acidobacteriota* phylum, increasing in abundance with depth and reaching 2.9% relative abundance in the 100–125 cm layer. Encoding the Wood-Ljungdahl pathway, SPRUCE 586 is a potential acetogen. Furthermore, *norB* was detected in this MAG, demonstrating its potential to produce N_2O, a potent greenhouse gas (Fig. 3). The family UBA7540, that contains SPRUCE 586, is among the most diverse families in the SPRUCE peat, with 17 species that are especially abundant in the deep peat (100–125 and 150–175 cm depths). However, only 35 UBA7540 genomes are found in GTDB and almost no information about this group is available in the literature. Thus, here we provide insights into the metabolic potential of this uncharacterized microbial group that abounds in the deep peat.

The *Bathyarchaeia* have been estimated to be among the most abundant soil microorganisms on Earth[56]. While more information is available from members of the phylum in marine sediments, the *Bathyarchaeia* were detected in a range of anoxic sediments, including peatlands (Woodcroft et al., 2018). Here we show, for the first time, that the *Bathyarchaeia* have the metabolic potential for sulfite reduction. Two MAGs belonging to the family FEN-987, SPRUCE 533 (0.07% mean relative abundance at 150–175 cm) and 422 (0.13% mean relative abundance at 100–125 cm), encode the corresponding hallmark genes. Interestingly, we observed the potential for oxygen, sulfite and nitrite respiration in SPRUCE 533, which highlights the adaptability of this species to variations in TEA availability (Fig. 3).

Similar to other well-studied peatlands in Europe, including Stordalen Mire[41], our previous work shows that genomes characterized as *Candidatus* Methanoflorens (Bog-38) are by far the most abundant methanogen genus present in SPRUCE soils[12]. The present study reveals that methanogens such as *Ca*. Methanoflorens may have a much more versatile metabolic potential than was previously

https://doi.org/10.1038/s41467-025-61664-7

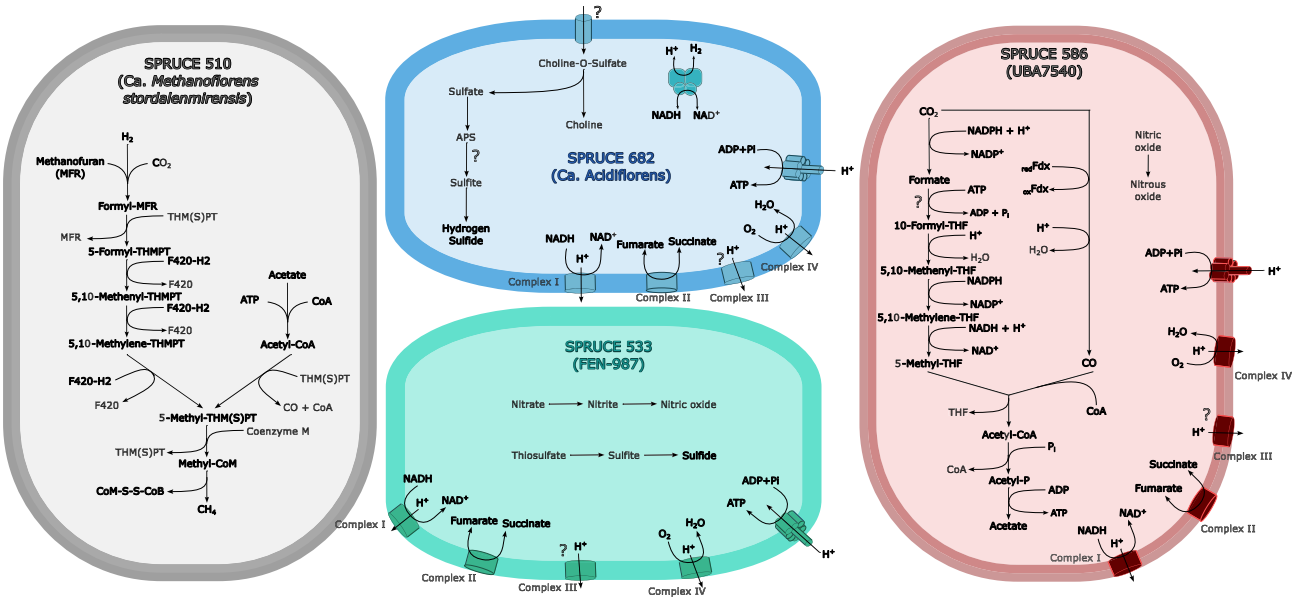

Fig. 3 | Dominant species in SPRUCE peat show a versatile metabolic potential. The metabolic potential of four abundant species is shown to highlight the capability of these species to adapt to the terminal electron acceptor availability. Question marks indicate enzymes or complexes that were not detected in the MAG but are likely to be present in the genome because the rest of the pathway in which they are involved was present. THMPT: Tetrahydromethanopterin; APS: Adenosine-5'-phosphosulfate; THF: Tetrahydrofolate; Fdx: Ferredoxin.

perceived. For example, *Ca*. Methanoflorens stordalenmirensis (SPRUCE 510), the most abundant *Ca*. Methanoflorens species in our dataset (2.8% average relative abundance at 40–50 cm), encodes the potential for both acetoclastic and hydrogenotrophic methanogenesis (Fig. 3). This dual potential was observed in 89.1% of the *Ca*. Methanoflorens MAGs ($n = 156$) recovered from both SPRUCE and Stordalen Mire, indicating that it is not an exclusive trait of SPRUCE 510 or assembly/binning error (chimeric genome), but a general feature of this genus. To date, members of *Methanosarcina*, a genus that is largely considered as acetotrophic, are the only methanogens known to utilize both hydrogen and acetate as substrates to produce methane[57].

Conceptual framework for depth-stratified metabolic potential in a temperate northern peatland

The primary environmental forcing we observe is the distinct depth stratification of microbial community composition (Fig. 1A, PERMANOVA p-value < 0.001) and functional potential (Fig. 4A), which closely mirrors changes in redox conditions, gas emissions, and soil organic matter composition (Fig. 4B, S4, S5). Redox chemistry drives microbial energy conservation pathways and is closely coupled to oxygen supply[58] linked to fluctuations in the water table, which rarely penetrates to below 30 cm depth at SPRUCE[45,59]. This strong depth stratification of microbial communities and processes is in agreement with our past studies at the SPRUCE site[28,32,60,61], those of other peatland systems[62–64] and as in our conceptual framework below, can be interpreted as a response of metabolic potential to changing terminal acceptor availability and soil organic matter quality.

In SPRUCE peat, sulfate reduction is an important metabolic trait throughout the depth profile, detected in 34 MAGs identified as sulfate reducers across *Acidobacteriota* (11 MAGs), *Desulfobacterota* (including Desulfobacterota_B and Desulfobacterota_G, 13 MAGs), and *Thermoplasmatota* (2 MAGs, in the genus UBA184). Sulfite reduction, on the other hand, is attributed to 20 MAGs distributed among *Acidobacteriota* (9 MAGs), *Desulfobacterota* (6 MAGs), and *Thermoproteota* (2 MAGs in the family Fen-987). Within the *Acidobacteriota*, a substantial proportion, 5% of this taxonomic group, have the potential to mediate sulfate reduction, while 4% have the capability to perform sulfite reduction. Overall, the keystone functional guild of methanogens constitutes 3% of all MAGs, and notably, 20 MAGs within this group ($n = 21$) exhibit the capability to execute multiple methanogenic pathways, further categorized into hydrogenotrophic (17 MAGs), acetoclastic (20 MAGs), and methylotrophic (6 MAGs) pathways (Data S3). The Wood-Ljungdahl pathway is common and phylogenetically diverse within our dataset; 58 bacterial MAGs, primarily from the phylum *Desulfobacterota* (15 MAGs), *Planctomycetota* (7 MAGs), *Acidobacteriota* (6 MAGs) and *Chloroflexota* (6 MAGs), show this potential. In addition, a large portion of the recovered *Thermoproteota* genomes contained the potential for homoacetogenesis (54.5% of the 33 identified MAGs). Note, however, that some species, such as sulfate-reducing bacteria, may use the reverse Wood-Ljungdahl pathway to generate energy through the oxidation of acetate to H_2 and CO_2[65]. Denitrification pathways are encoded by 174 MAGs, representing 25% of all MAGs, with *Bacteria* and *Archaea* contributing 160 and 14 of these MAGs, respectively. Members of the *Acidobacteriota* are significant players in denitrification, with 48 MAGs (21.6% of all *Acidobacteriota* MAGs, Fig. S6) containing this potential, while *Desulfobacterota*, including Desulfobacterota_B and Desulfobacterota_G, contribute 23 MAGs, making up 46.7% of all *Desulfobacterota* involved in denitrification (Fig. S7).

The acrotelm (10–20 cm): fluctuations in conditions lead to a diverse aerobic and fermentative microbial community

Peat mosses (*Sphagnum* spp.) carpet the soil surface in many temperate peatlands, including the S1 bog at SPRUCE sampled here. Beneath the living *Sphagnum* layer and above the water table, the 10-20 cm depth interval stands out as a hotspot for decomposition (Fig. S8), as SOM derived from decaying plant biomass and labile organic compounds from root exudates are decomposed primarily via aerobic respiration. Our previous work showed that molecular oxygen is available at this depth[61]. Accordingly, MAGs encoding for pathways of aerobic respiration dominate at this depth (Fig. S8). Fungi, which are

https://doi.org/10.1038/s41467-025-61664-7

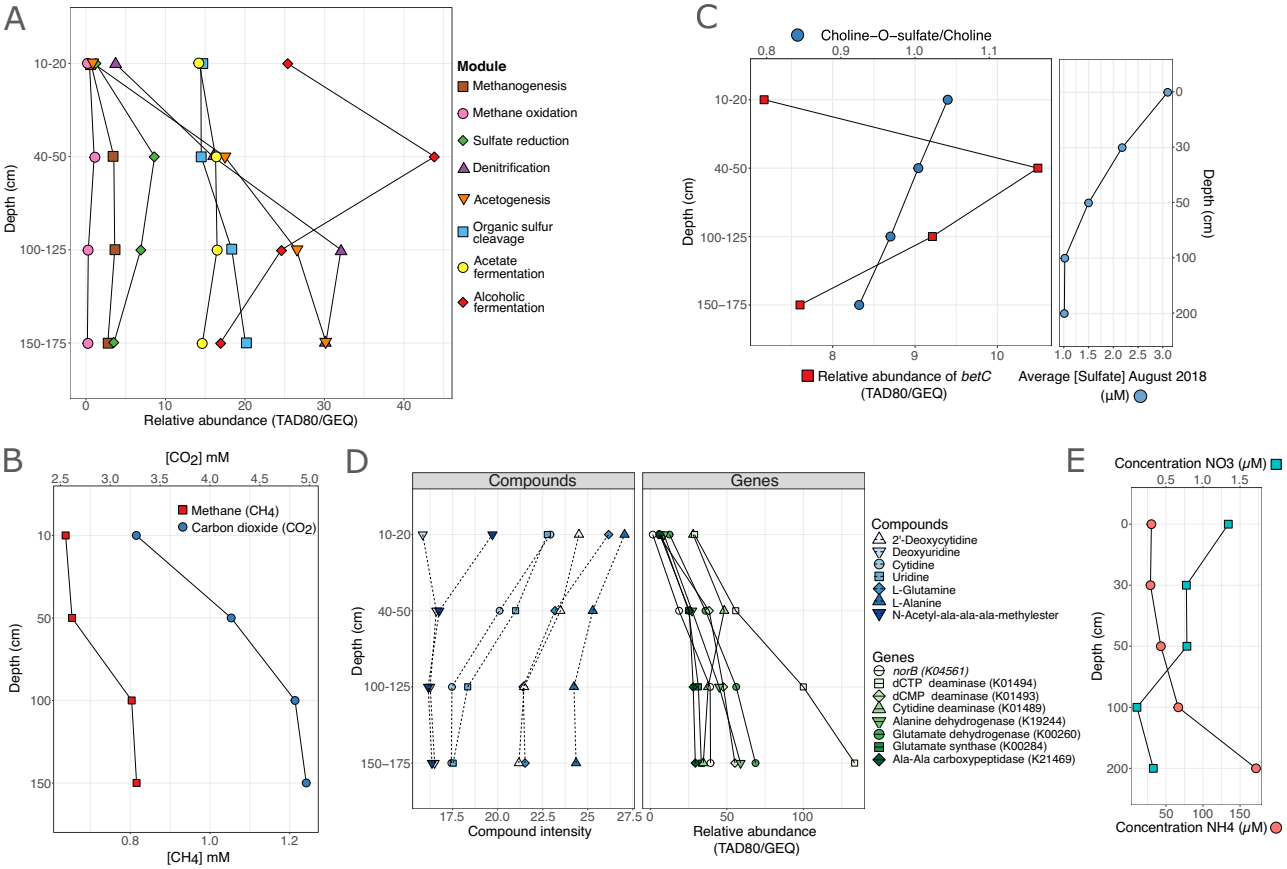

Fig. 4 | Relative abundance of metabolic pathways along with concentrations of organic compounds and TEAs across the depth profile supports organic matter cleavage as a source of TEA. A Mean aggregated relative abundance (TAD80/GEQ, x-axis) of MAGs encoding each metabolic pathway (module) along the depth profile (cm, y-axis). Each color and shape combination correspond to one metabolic pathway. 10–20 $n = 34$; 40–50 $n = 34$ 100–125 $n = 32$; 150-175 $n = 31$. **B** Concentration of greenhouse gases CO_2 (mM, top x-axis, blue circles) and CH_4 (mM, bottom x-axis, red squares) along the peat column (cm, y-axis). **C** On the left, ratio of Choline to Choline-O-sulfate (intensity, top x-axis, blue circles) and the mean aggregated relative abundance of *betC* (TAD80/GEQ, bottom x-axis, red squares), along the peat column (cm, y-axis). On the right, sulfate concentration in porewater (μM, x-axis) through the depth profile (cm, y-axis). **D** The intensity of compounds and the relative abundance of genes (TAD80/GEQ for genes and intensity for compounds, x-axis) related to deamination are depicted along the peat column (cm, y-axis). Each color and shape combination correspond to the depth profile of one gene or compound. **E** concentration of nitrate (NO_3, μM, top x-axis, blue squares) and ammonium (NH_4 μM, bottom x-axis, red circle) through the depth profile (cm, y-axis).

either strictly aerobic or yeast capable of fermentation, have been also shown to peak in abundance[61] and richness in this oxic/anoxic zone[66]. We did not identify clear trends in the overall response of aerobes to warming (Fig. 2A) and only a few aerobic genomes showed a positive (2 MAGs) and negative (4 MAGs) response to warming (Data S2), indicating a lack of response of this functional group to warming treatment.

The S1 bog water table occasionally reaches the 10 to 20 cm layer below surface and our previous work shows that oxygen is depleted where the soil is saturated with water[61]. Thus, the surface peat is ephemerally anoxic, and we find a high metabolic potential for acetate and alcoholic fermentation in the acrotelm (Fig. 4A, S8), indicating heterotrophy is mainly driven by fermentation under anoxic conditions. In agreement with this observation, St James et al. (2020) detected the potential for acetate fermentation in most MAGs present in the 10–40 cm layer from the *Sphagnum*-dominated MacLean bog (New York State). In the present study, acetate production via fermentation is encoded mainly in the phyla *Verrucomicrobiota* (14 MAGs) and *Actinomycetota* (12 MAGs), while the potential for alcoholic fermentation was present in *Acidobacteriota* (165 MAGs), *Actinomycetota* (48 MAGs) and *Pseudomonadota* (46 MAGs). The total relative abundance of MAGs with the potential to ferment to acetate and alcohol did not respond to warming, and the response of MAGs capable of fermentation in the surface was mixed (Data S2).

In the acrotelm, aerobic respiration is coupled to canonical methanotrophy at the oxic-anoxic interface where oxygen and methane are supplied from above and below, respectively. Anaerobic respiration pathways are less pronounced at this depth, with the genomic potential for methanogenesis, sulfate respiration, and acetogenesis at their lowest abundances (Fig. 4A). Nevertheless, these anaerobic pathways are still notably active (Fig. 5A), and the increase in porewater gas concentration in response to temperature[12] indicates that these pathways are sensitive to climate change drivers. We find evidence that the dominant methanogen at SPRUCE, *Ca*. Methanoflorens, is actively performing both acetoclastic and hydrogenotrophic methanogenesis at the surface of the bog (Fig. 5B). Other active methanogens, such as members of the genus *Methanobacterium* and *Methanoregula*, are also capable of flexibility in their substrate use. Considering the widespread metabolic flexibility of methanogens at SPRUCE, the significant increase in ribosomal protein transcription ($P = 0.009$) in the most active acetogens of the surface layer (Fig. 5C) suggests that the mechanism by which elevated temperatures promote methanogenesis in the bog is through enhanced availability of substrates (e.g., acetate).

https://doi.org/10.1038/s41467-025-61664-7

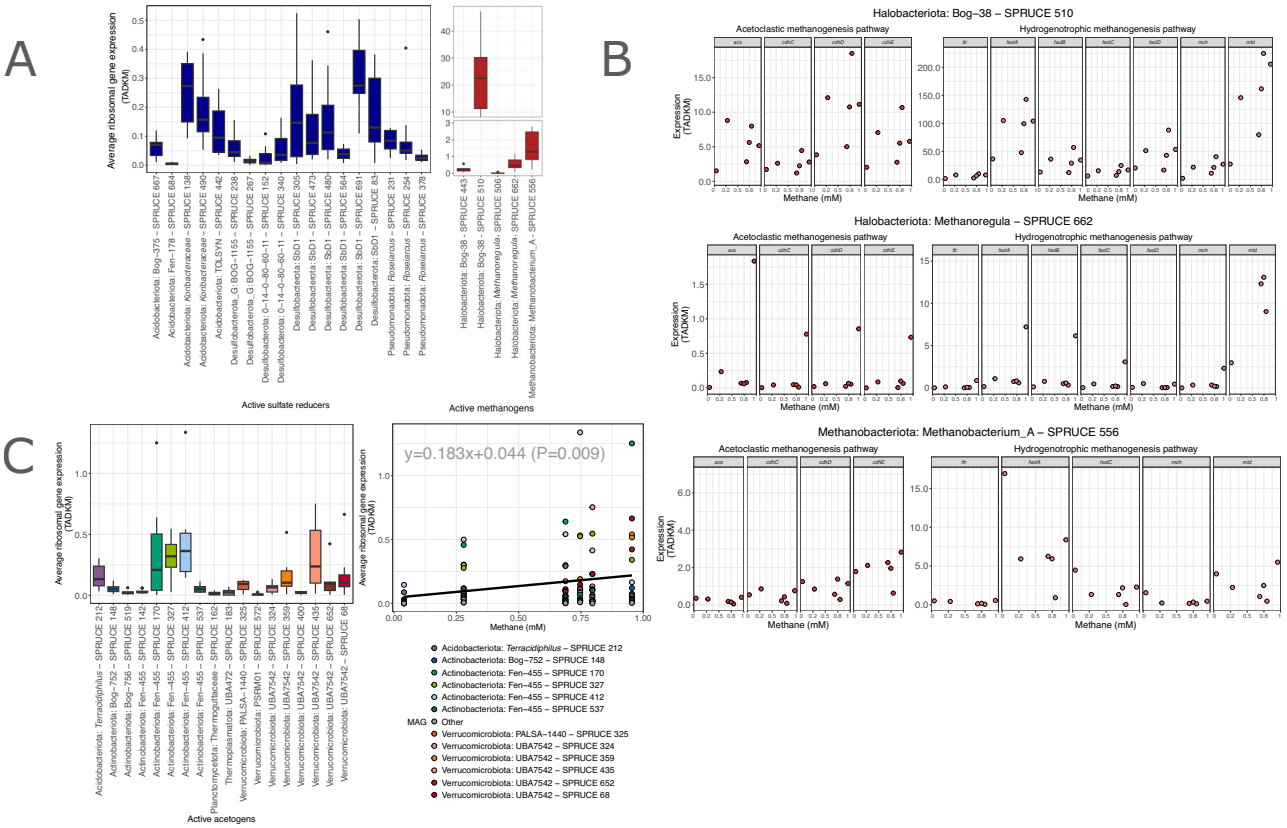

Fig. 5 | Acetoclastic and hydrogenotrophic methanogenic pathways are expressed simultaneously in the same MAG and methanogenesis responds to increasing activity of acetogenic bacteria. A Average ribosomal protein expression (trimmed average depth per kilobase per million reads, y-axis) of MAGs expressing the module for sulfate reduction (red) and methanogenesis (blue) (x-axis). Each box displays distribution of MAG-specific expression in surface depth in each enclosure using interquartile ranges, with the rectangle (box) delineating the data within the 25–75th percentile. The median (50th percentile) is displayed as a horizontal line within the box. Values below the 25th or above the 75th percentiles are shown with a whisker below and above the box, respectively. Extreme values are considered outliers and shown as individual dots. **B** Gene expression for genes in the acetoclastic methanogenesis pathway (red) and the hydrogenotrophic methanogenesis pathway (pink) measured as trimmed average depth per kilobase per million reads (y-axis) across methane production (mM, x-axis) for the three most active methanogens (each row displays the data for one MAG). *acs*: acetyl-CoA synthetase; *cdhC*: acetyl-CoA decarbonylase/synthase, CODH/ACS complex subunit beta; *cdhD*: acetyl-CoA decarbonylase/synthase, CODH/ACS complex subunit delta; *cdhE*: acetyl-CoA decarbonylase/synthase, CODH/ACS complex subunit gamma; *ftr*: formylmethanofuran--tetrahydromethanopterin N-formyltransferase; *fwdA*: formylmethanofuran dehydrogenase subunit A; *fwdB*: formylmethanofuran dehydrogenase subunit B; *fwdC*: formylmethanofuran dehydrogenase subunit C; *fwdD*: formylmethanofuran dehydrogenase subunit D; *mch*: methenyltetrahydromethanopterin cyclohydrolase; *mtd*: methylenetetrahydromethanopterin dehydrogenase. **C** Average ribosomal protein expression (trimmed average depth per kilobase per million reads, y-axis) of MAGs expressing the Wood-Ljundhal pathway of acetate production (left x-axis) and over the methane production (mM, right x-axis). On the left plot, each box displays data distribution using interquartile ranges, with the rectangle (box) delineating the data within the 25–75th percentile. The median (50th percentile) is displayed as a horizontal line within the box. Values below the 25th or above the 75th percentiles are shown with a whisker below and above the box, respectively. Extreme values are considered outliers and shown as individual dots. Colors indicate the MAG activity being depicted, and black line shows the overall significant trend of a two-sided linear regression predicting the average ribosomal protein expression of a MAG expressing the Wood-Ljundhal pathway of acetate production with increasing porewater methane concentration (P = 0.009, n = 108). P-value was derived from the model coefficients, with no adjustments for multiple comparisons applied.

The mesotelm (40–50 cm): hot spot of anaerobic respiration via cleavage of TEAs from organic matter

Peatlands store the majority of their carbon in thick peat layers below the water table, where soil organic matter decomposition is dominated by anaerobic pathways[20,21,28,58]. Within the 40–50 cm depth range at SPRUCE, the potential for aerobic processes diminishes, giving way to anaerobic respiration as the primary driver of organic matter degradation (Fig. 4A and S8).

The paradigm in freshwater wetlands is that methanogenesis predominates over the TEA pathways coupled to the decomposition of SOM[20,21,33,35,58], thereby regulating the production of greenhouse gases (CO_2, CH_4). Here, however, despite a peak in methanogen abundance at 40-50 and 100-125 cm, the potential for other anaerobic respiration pathways (as reflected by relative abundance of the corresponding hallmark genes), such as sulfate reduction, exceeds that of methanogenesis (Fig. 4A). We find that sulfate-reducers are less active individually, but unlike methanogens, which are almost monospecific in their activity, a diverse set of sulfate-reducers are active (Fig. 5A). The stoichiometry of methanogenesis predicts a 1:1 ratio of CO_2 to CH_4 production and higher ratios of CO_2:CH_4 implicate alternate carbon oxidation pathways[23,28,33]. Despite the scarcity of inorganic TEAs in peat, numerous field and incubation studies in northern peatlands, including those conducted at SPRUCE, have consistently reported 10 to 1,000 times higher CO_2 production than CH_4, indicating the dominance of alternative TEAPs in SOM decomposition[11,23,28–32]. Our results provide further support for these observations (Fig. 4B) but raise the question of the source of TEAs supporting anaerobic respiration, which are typically detected at very low concentrations in peat[67,68].

We propose that inorganic TEAs are obtained from the cleavage of the organic matter itself. Indeed, of the sulfate- and sulfite-reducers detected, 46 out of 55 MAGs demonstrate the genomic

potential to cleave inorganic sulfur (sulfate, sulfite) from organic-sulfur compounds (Figure S9). This ability is widespread throughout the total microbial community, with 31% of our MAGs encoding genes for inorganic sulfur cleavage. Sulfur cleavage from organic matter is independent of oxygen regime[69] and persists throughout the depth profile (Fig. 4A), suggesting that TEAs are cleaved from organic matter. Further, our data suggest that choline-O-sulfate, shown to be a major metabolite produced by *Sphagnum*[70], is likely an important source of sulfate for anaerobic respiration, as the abundance of *betC* genes, responsible for cleaving SO_4^{2-} from choline-O-sulfate, correlates with the ratio choline/choline-O-sulfate as well as porewater SO_4^{2-} concentrations through the depth profile. Specifically, *betC* decreases in relative abundance in parallel with the abundance of detected choline-O-sulfate within our companion metabolite dataset and a relative increase in the byproduct, choline (Fig. 4C). Similarly, porewater SO_4^{2-} concentrations follow the decrease in *betC* abundance supporting the link between them. Throughout the growing season, we observed that porewater SO_4^{2-} concentration appears to be mainly driven by microbial activity regulated by water table rather than by the amount of rainwater (Fig. S10). Under oxic conditions (low water table), porewater SO_4^{2-} concentration increases, likely because of a higher degradation activity, while under anoxic conditions (high water table), SO_4^{2-} concentration decreases due to the activity of sulfate-reducers. It should be noted that micromolar concentrations of SO_4^{2-} are sufficient to support sulfate reduction activity in peat soils[71]. Gene expression of *betC* in the acrotelm confirms the activity of the gene and its involvement in sulfur cycling (Fig. S11). *BetC* releases SO_4^{2-} transiently, as *betC* expression and SO_4^{2-} are not significantly correlated, but gene expression is intricately related to the intensity of its substrate, choline-O-sulfate and its other product, choline. The expression of *dsrA* is significantly negatively correlated with SO_4^{2-} (Estimate = -0.005, $P = 0.005$) and choline concentrations (Estimate = -0.025, $P = 0.001$), indicating that when SO_4^{2-} accumulates under oxic conditions, *dsrA* transcripts decrease and choline accumulates. Choline-o-sulfate, however, does not significantly relate to the rate of *dsrA* expression (0.096), since only some MAGs respond to choline-O-sulfate in the peat (Fig. S11). These lines of evidence suggest that bacteria capable of sulfate cleavage from organic matter are supplying sulfate as an alternative source of TEA for respiration. Thus, our findings provide a possible explanation for the long-standing question of the mechanisms behind the unexpectedly high CO_2 production in TEA-poor peatlands.

Our previous determinations of microbial activity corroborate the observations of genomic functional potential reported here, revealing a mid-depth hotspot in organic matter decomposition activity at 40–50 cm in the peat column, as evidenced by rates and ratios of greenhouse gas production, the accumulation of gases in soil porewaters, and the transformation of SOM (metabolomes) with depth[11,12,32,39,60]. While relative gene abundance provides compelling evidence for the importance of the metabolic potential of anaerobic respiration pathways at depth, our hypotheses must be confirmed by process-specific rate measurements in the future. Nevertheless, this potential mechanism of organic matter processing has implications for warming peatlands, and could explain increases in porewater CO_2 observed below the water table[12]. Although warming did not impact the total relative abundance of MAGs with the potential to reduce sulfate, sulfite (Fig. 4B), or cleave sulfate from organic matter, among the five genomes that significantly increase in relative abundance with warming at 40–50 cm depth, two are *Acidobacteriota* involved in sulfur cycling (Data S2). The first, SPRUCE 490 in the family *Koribactericeae* (Coefficient = 1.084, $P = 0.035$), has the genomic potential to reduce sulfate and sulfite and ferment to alcohol. The second, SPRUCE 69, in the family *Bryobacteraceae* (Coefficient=1.650, $P = 0.45$), can potentially cleave sulfate from choline-O-sulfate.

The catotelm (100–125 and 150–175 cm): interactions between methanogens and acetogens as well as high potential for denitrification and methylotrophic methanogenesis

Below the mid-depth peak (40–50 cm) in anaerobic respiration activity, the genomic potential for acetogenesis via the Wood-Ljungdahl pathway continues to increase, resulting in the highest concentrations of acetate in the deep peat (Fig. 4A, Fig. S12). While metaproteomic data from the catotelm is not available, key enzymes in the Wood-Ljungdahl pathway, such as acetyl-CoA synthase and 5-methyltetrahydrofolate corrinoid/iron sulfur protein methyltransferase, were consistently detected between 20–70 cm depth, providing evidence for the activity of this pathway. The pathways of methanogenesis are not partitioned equally throughout the depth profile, and although methanogens with the potential to produce methane via the acetoclastic and hydrogenotrophic pathways dominate throughout the peat profile, methylotrophic methanogens increase noticeably in the deep peat (Fig. S13). Methylaminated organic compounds, such as 1-methyladenine and 1-methylguanine are negatively correlated (r = -0.84, and r = -0.84) with the abundance of the gene *mttB*, which encodes for a trimethylamine co-methyltransferase. The depletion of metabolites in the presence of key genes in the pathway of methylaminotrophic methanogenesis suggests that the pathway is active and links the deep peat to the complex, organic bound nitrogen cycle of peatlands. Known substrates for methylotrophic methanogenesis include trimethylamines, dimethylamines, monomethylamines, glycine betaine, dimethyl sulfide (DMS), methanol, and choline, among others[72]. In SPRUCE peat, methanol and choline are likely derived from the degradation of lignin and choline-O-sulfate, respectively, providing key substrates for methylotrophic methanogenesis, as recently proposed for the Stordalen Mire[44]. Furthermore, the observed negative correlation between methylnucleotides and *mttB* suggests that methylated nucleotides may potentially act as precursors for methylamines, a hypothesis that warrants further investigation. Of the few genomes that significantly respond to warming, SPRUCE 117 in the order *Methanomassiliicoccales*, which has the potential to produce methane using acetate, methanol, or methylamine as substrate, is negatively correlated with temperature in the deep peat (100-125 cm: Coefficient = -0.380, $P = 0.042$, and 150-175 cm: Coefficient = -2.206, $P = 0.020$). Recently, methylotrophic methanogenesis has emerged as an important process in peatland soils, with reports of methylotrophic orders accounting for up to half of the transcription[44]. In the bog where our experiment was conducted, ^{13}C-labeled methylated substrates including methanol and monomethylamine were readily converted to CH_4 by methylotrophic methanogens[73]. The negative correlation of SPRUCE 117 relative abundance with warming signals that methanogenesis pathways at SPRUCE are shifting with warming, but the decrease in metabolic potential for the demethylation of methylaminated organic compounds cannot explain why the bog is becoming more methanogenic with warming.

The deep peat exhibited significant metabolic potential for denitrification, with a peak occurring at 100-125 cm depth, which coincided with a consistent depletion of NO_3^- at this depth (Fig. 4A, E). Metaproteomic data throughout the depth profile and transcripts from the acrotelm confirmed the expression of denitrification genes. We observed a distinct distribution of genes involved in denitrification, with *norB* showing by far the highest relative abundance (Fig. S14). This gene encodes the nitric oxide reductase, an enzyme that catalyzes the reduction of nitric oxide (NO) to the potent greenhouse gas nitrous oxide (N_2O), pointing to the catotelm as a potential source of N_2O. Given the limited availability of oxidized nitrogen compounds in peat, the origin of the terminal electron acceptors for denitrification remains unclear. We propose that inorganic nitrogen forms could be derived from the organic matter itself, akin to sulfur compounds. Several lines of evidence from our metagenomic and metabolomic

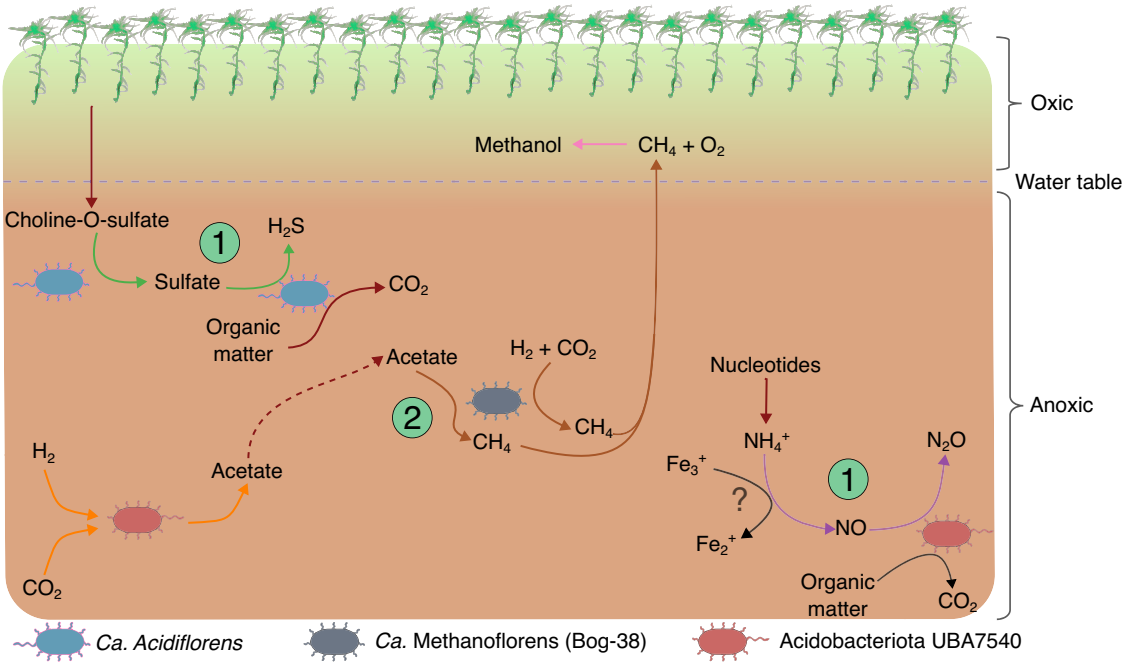

Fig. 6 | Conceptual model of terminal steps of organic matter degradation in peatlands. Simplified model of the main terminal electron-accepting pathways driving carbon turnover in SPRUCE peat based on the data shown in Figs. 3–5. Arrow colors follows the same schema as in Fig. 4A. Dashed lines show indirect interactions while question marks point to reactions that could hypothetically be taking place in SPRUCE peat based on literature and genomic potential. 1) Cleavage of organic matter (choline-O-sulfate and nucleotides) to obtain TEA to fuel anaerobic respiration. 2) Metabolic versatility of methanogens with the capability to perform both acetoclastic and hydrogenotrophic methanogenesis.

data support this hypothesis. Genes related to the hydrolysis and deamination of organic nitrogen compounds correlate positively with *norB*, while the respective compounds (e.g., nucleosides, peptides and amino acids) correlate negatively, suggesting consumption (Fig. 4D). In agreement with this observation, we found peptidases encoded close to the *norB* genes (i.e., within 10 genes upstream or downstream) in 54% of all *norB*-encoding MAGs, which suggests that these genes may act on the same pathway. In addition, previous metabolomic studies at SPRUCE reported an enrichment of N compounds with depth[32]. However, the potential for reoxidation or recycling of inorganic nitrogen in the deep, anoxic peat remains enigmatic. Mineralized nitrogen is generally released in a reduced form as ammonium, and accordingly, porewater ammonium concentration in SPRUCE increases with depth (Fig. 4E). Possible explanations for the oxidation of ammonium in anaerobic peat soils include Fe(III)-mediated anaerobic ammonium oxidation (Feammox)[74,75], or ammonium oxidation by methanotrophs[76]. While little information is available, biogeochemical evidence indicates Feammox is favored under acidic, anoxic conditions[75], which match the chemical environment in SPRUCE peat. Although Fe(III) concentrations at SPRUCE are low in comparison to mineral soils, a substantial pool of Fe(III) is observed that decreases with depth, reaching a minimum concentration at the 150–175 cm depth interval[77]. Indeed, we observed a strong correlation in the relative abundance of *norB* and ferritin genes (Pearson's correlation=0.83; p-value = 0), supporting a close relationship between them (Fig. S15). Thus, these trends are consistent with our hypothesis that Fe(III) could be used as the electron acceptor in the oxidation of ammonium. Decomposition rates are shown to decline dramatically between 50 and 100 cm depth[22,32], and an alternate explanation is simply that the cleavage of some oxidized organic S and N compounds supplies sufficient inorganic TEAs to support the lower rates of anaerobic respiration, and the replenishment of electron acceptor through reoxidation is not necessary.

Our ability to predict the impact of climate change on the vast carbon stores of peatlands is hampered by a limited understanding of the microbial dynamics and metabolic pathways that regulate carbon turnover. Here, we contribute to filling this gap by providing a conceptual framework for the functional potential of microbial communities extending 2 m into the peat column. The genome-resolved findings presented here provide an explanation for field observations that peatlands generally emit much more CO_2 than CH_4 under anaerobic conditions and propose mechanisms by which warming can impact the metabolism of the microbial community. Our conclusions on microbial dynamics in the belowground peat are supported by over 10 years of biogeochemical and metabolomics data collected from the SPRUCE site[11,12,23,39,60,61,77,78]. From our conceptual framework, we describe two potential mechanisms that could explain why microbial community composition remains stable despite increasing greenhouse gas emissions in the face of warming temperatures (Fig. 6).

First, the wide metabolic versatility of abundant species, may allow them to adapt their activity without significantly changing their abundance. For example, *Ca.* Methanoflorens (Bog-38) species, exhibit a genomic repertoire capable of performing both acetoclastic and hydrogenotrophic methanogenesis, and *Ca.* Methanoflorens is actively performing both acetoclastic and hydrogenotrophic methanogenesis at the surface of the bog. Thus, these versatile methanogens can take advantage of the available acetate, or if acetoclastic methanogenesis is not energetically favorable, use the CO_2 and H_2 produced from the oxidation of energetically rich substrates for hydrogenotrophic methanogenesis (Fig. 6)[79]. This metabolic versatility combined with the slow growth rate of methanogens[80,81] and the influence of temperature on microbial activity, may explain why biogeochemical data show that methanogenic activity increases with warming, but community composition remains stable. A transition between methanogenic pathways with increasing temperature is indeed expected, based on previous isotopic measurements in the SPRUCE peat that indicated a shift from hydrogenotrophic to acetoclastic methanogenesis[12]. However, validation of such a transition in response to climate change drivers necessitates further experimental evidence from activity-based (metatranscriptomic) studies.

Second, the increased input of organic matter resulting from higher plant productivity at warmer temperatures may replenish the TEA pool available for anaerobic respiration, given the potential capability of peat microbes to obtain TEA from organic compounds (Fig. 6). This mechanism could thus be facilitating the respiration of organic matter via alternative pathways to methanogenesis and thus, acting as a counterbalance to limit the growth and activity of methanogens by fostering the activity of other anaerobic groups (e.g., sulfate-reducers) and thus, the release of CO_2. The genomic evidence reported here in support of this mechanism is further complemented by previous studies that showed that TEA limitation is alleviated at high temperatures[23,35]. Further experimental data will be required in the future to assess the existence and extent of this mechanism. For example, the activity of enzymes responsible for the cleavage of TEA from organic compounds, such choline-sulfatase (*betC*), would be expected to correlate with the release of CO_2. Culture studies will also be needed to verify these physiological mechanisms.

To conclude, we have assessed the impact of warming on keystone functional guilds, providing evidence that microbial community composition in northern peatlands is resistant despite the sensitivity of gas production[46]. Therefore, the previously reported increase in CH_4 and CO_2 is likely due to changes in microbial activity rather than community changes. The uncovered taxonomic and metabolic novelty of microbes inhabiting peat soils along with our proposed conceptual model alter perceptions of anaerobic respiration pathways mediating terminal decomposition in peatlands and provide a mechanistic framework for improved predictions of the ratio of CO_2:CH_4 emissions and their likely response to climate drivers.

Methods

Study site

The Spruce and Peatland Responses Under Changing Environments (SPRUCE) is a whole ecosystem warming experiment located in the ombrotrophic, acidic S1 Bog of the Marcell Experimental Forest, north of Grand Rapids, MN (47°30.4760 N; 93°27.1620 W). The experiment consists of 17 open-top chambers that control the peat and air temperature (ambient, +0, +2.25, +4.5, +6.75 and +9 °C) as well as atmospheric CO_2 concentration (ambient and 900 ppm). In June 2014, an array of heating rods 3 m in depth were established and began warming the belowground peat. A subsurface corral hydrologically isolates each enclosure but allow natural lateral water flow. In August 2015, aboveground air warming was initiated. The air within the enclosure is heated by a propane heater outside the chamber and reintroduced to achieve desired temperature levels, with monitoring conducted at the target control point located at +2 meters in the center of the plot. In 2016, CO_2 additions began. The pure CO_2 is vaporized and warmed before being distributed and homogenized within the enclosure[82]. Environmental variables such as temperature, precipitation and gas emissions are constantly monitored. The readers are referred to the official webpage for further information on the experiment and a comprehensive list of project measurements (https://mnspruce.ornl.gov).

The outflow chemistry from the enclosures indicates that, in August 2016 and 2018, on average the pH was 3.42 and total organic carbon was 85.83 mg C/L. Porewater chemistry data and environmental monitoring data was accessed on the SPRUCE repository[83,84]. The S1 Bog is dominated by peat mosses of the genus *Sphagnum*, including *S. fallax* and *S. divinum* (previously *magellanicum*), and sparsely populated by Black spruce (*Picea mariana*) and larch (*Larix laricina)*. Ericaceous shrubs such as *Rhododendron groenlandicum* and *Chamaedaphne calyculata* are commonly found throughout the peatland and accompanied by the herbaceous *Maianthemum trifolium*. In the absence of severe drought conditions, the water table fluctuates at a depth of between 0 and 30 cm of peat depth[45,61,78,85,86].

Physicochemical measurements

Porewater concentrations of SO_4, NH_4 and NO_3 were collected from the SPRUCE data repository[84]. This data was collected at regular intervales of twice or three times per month during the ice-free period of the year. Daily precipitation data was obtained from Sebestyen et al.[87]. Acetate concentration along the depth profile was obtained from Zalman et al.[73].

DNA and RNA extraction and sequencing

Peat samples were collected in June of 2015 and 2016 and August of 2018 from the hollows of each of the 10 whole-ecosystem warming chambers with a serrated knife at the surface and a Russian corer at depth. The samples were separated into depth increments and six 0.35 g subsamples of homogenized peat from the 10–20 cm, 40–50 cm, 100–125 cm, and 150–175 cm depth increments were collected and extracted for DNA using the MoBio PowerSoil Pro Kit (QIAGEN) and resuspended in 50 µL of 10 mM Tris buffer. Illumina TruSeq metagenome libraries were generated by the JGI using their standard protocol. Metagenomes are publicly available on the JGI Genome Portal and NCBI Sequence Read Archive (SRA) (Data S4). We obtained peat samples in August 2020 from the hollows of each of the 10 whole-ecosystem warming chambers from the 10–20 cm depth increment. Sample was homogenized, and subsamples of 20 mL were flash frozen and kept at -80 °C for RNA extractions. We extracted RNA from six subsets of 30 mg of soil from the 10–20 cm depth using the Powermicrobiome RNeasy kit (QIAGEN), purified the samples using the OneStep PCR Inhibitor Removal Kit (ZYMO), digested the DNA using TURBO DNA-free Kit (Invitrogen), and pooled the samples with RNA Clean & Concentrator-5 (ZYMO).

Metagenome preprocessing, binning and annotations

Metagenomic reads were quality filtered using bbduk.sh v38.18 (qtrim = w,3 trimq = 17 minlength = 70 tbo tossjunk = t cardinalityout = t)[88] and then, coverage was normalized using bbnorm.sh v38.18 (target=30 min=5 prefilter=t tossbadreads=t). Both original and normalized metagenomic reads were assembled independently with idba_ud v1.1.3 (--maxk 120)[89] and SPAdes.py v3.15.5 (-k 21,33,55,77,99,127 --meta --only-assembler)[90]. Then, contigs longer than 1 kb were used to recovery metagenome-assembled genomes (MAGs) with Maxbin v2.2.7[91] and metaBAT2 v2.15[92]. MAGs were first dereplicated (within samples) with miga v1.3.8.3 (derep_wf --fast)[93] yielding a total of 5,963 MAGs that were further dereplicated (between samples) using dRep v3.4.3 (-comp 50 -conn 15 -sa 0.95 --S_algorithm fastANI)[94]. As a result, the final dataset was composed of 697 unique genomospecies. CheckM v1.2.2 (lineage_wf)[95] was employed to assess MAG quality and GTDB-tk v2.1.0 (classify_wf)[96] to classify them taxonomically. MAG annotation was performed with DRAM v1.4.6 using default parameters[97] and KEGG module completeness was evaluated using a custom R script. Pathways were then manually curated for each MAG, using pathway-specific criteria to determine if a MAG had the metabolic potential for the pathway (see Data S5 for criteria used to define presence/absence of each metabolic pathway). In general, pathways were considered as detected when at least half of the genes in the KEGG pathway and a key gene in the pathway (e.g. *dsrA* for sulfate reduction, *fdh* for the Wood–Ljungdahl pathway) were annotated. The potential metabolic pathways for each MAG are available in Data S7. We determined MAG active function using the same definition but replaced MAG gene presence with metatranscriptomic coverage of MAG genes. To determine MAG-specific activity, we calculated average ribosomal protein activity, and excluded MAGs that did not express at least half the ribosomal proteins listed in Data S6. CoverM v0.6.1[98] was employed to calculate the truncated average sequencing depth at 80% (TAD80) for each MAG (-p bwa-mem --min-read-aligned-length 100 --min-read-percent-identity 95 --min-read-aligned-percent 70 --exclude-supplementary -m trimmed_mean --trim-min 10 --trim-max 90). TAD80 was then

normalized by genome equivalent values obtained from MicrobeCensus v1.1.0[99] to normalize coverage by the sequencing depth while accounting for microbial genome size within the sample. MAGs analyzed in this manuscript were deposited in NCBI under BioProject PRJNA1084886.

Phylogenomic tree

Proteins encoded on each MAG were first predicted using Prodigal v2.6.3 (-p meta)[100].Then, PhyloPhlAn v3.0.67 was used to build a phylogenomic tree based on the alignment of 400 universal gene markers[101](--diversity high --fast). The tree was finally drawn and annotations added using ggtree[102].

Metatranscriptomic read processing

We quality filtered the metatranscriptome using JGI's BBTools toolkit (Bushnell B., 2015) and removed rRNA reads using sortMeRNA v.4.3.4[103]. We assessed DNA contamination in metatranscriptomic samples using custom scripts as in Johnston, et al.[104]. We used CoverM v0.6.1[98] to calculate the truncated average metatranscriptomic sequencing depth at 80% of each gene and normalized by sampled depth as kilobase per million mapped reads using quality filtered metatranscript library size (TADKM).

Comparison to genomes retrieved from representative global soil types

The largest metagenomic dataset from northern peatlands published to date was obtained from Stordalen Mire in Sweden[47]. To assess how different or similar our metagenomes are to Stordalen Mire metagenomes, approaches at both the read level and the MAG level were performed. At the read level, MASH v1.1[105] distances were calculated (sketch -s 10000 -r -m 2) and plotted on an Non-metric Multi-Dimensional Scaling (NMDS) plot on R using the vegan[106] and ggplot packages[107]. At the MAG level, all MAGs publicly available from Stordalen Mire[47] were retrieved and dereplicated using dRep, as explained above. Then, ANI between dereplicated Stordalen Mire and SPRUCE MAGs (1,645 and 697 MAGs, respectively), was calculated with fastANI v1.33[108].

To compare SPRUCE genomes to those from a variety of representative soils around the world, metagenomes from upland forest (Hubbard Brook Experimental Forest)[109], Antarctic[110], tropical[110], grassland[111], agricultural soils[112] as well as peat incubation samples from Ward reservation soils (Massachusetts, USA)[38] were retrieved from the SRA (Data S8). MASH distances were calculated, as explained above, and 3D NMDS plots were drawn with the plotly R package[113].

Gene abundances

Genes and proteins were predicted from all contigs longer than 1 kb recovered from the 131 metagenomes using Prodigal v2.6.3 (-p meta). MMseqs2 v13.45111[114] was employed to obtain a non-redundant gene database (easy-cluster -c 0.8 --cov-mode 0 --min-seq-id 0.95) which was then used by CoverM v0.6.1 to calculate gene sequencing depth (-p bwa-mem --min-read-percent-identity 95 --min-read-aligned-percent 50 --exclude-supplementary -m mean --min-covered-fraction 80 --contig-end-exclusion 20). The non-redundant gene ids were extracted from the protein file using FastA.filter.pl from the enveomics package[115] to get the non-redundant protein database which was annotated with kofamscan[116], and the output filtered to keep only hits with evalue < 1e-15 and scores >90% of the precomputed scores. Gene sequencing depth and annotation data was merged with Table.merge.pl and the table parsed with custom R scripts to get the KO sequencing depth per sample. Finally, KO relative abundances were obtained by dividing the KO sequencing depth by genome equivalents.

Metabolomics

Metabolomics analysis was performed on 40 wet peat samples (10 enclosures, 4 depth per enclosure, 1 replicate per depth and enclosure) collected in 2018 that were also used for metagenomic analysis. To dry samples and ensure uniform starting weight for extraction, peat samples were first lyophilized using a Labconco FreeZone, Benchtop freeze dryer for 48 h. The freeze-dried peat samples (0.2 g) were extracted by adding 20 mL of an 80:20 solution of MeOH: sterile MilliQ water. Samples were briefly vortexed and sonicated in a water bath for 2 hr at 20 °C (FisherBrand CPX3800). The supernatant was filtered through a 0.45 um filter to remove cellular debris and plant material. Of this extract, 7 mL were transferred to two glass autosampler vials (3.5 mL each), dried in a vacuum centrifuge (Eppendorf Vacufuge plus), and stored at −80 °C. Prior to CL-MS/MS analysis, samples were reconstituted in 80:20 water:methanol for reverse phase (RP), and 50:50 water:acetonitrile for hydrophilic interaction liquid chromatography (HILIC).

Liquid chromatography-tandem mass spectrometry (LC-MS/MS)

Liquid chromatography was conducted using a Thermo Scientific Vanquish Duo ultra-high performance liquid chromatography system (UHPLC). For reverse phase (RP) separation, extracts were separated on a Waters ACQUITY HSS T3 C18 column, while hydrophilic interaction liquid chromatography (HILIC) separation utilized a Waters ACQUITY BEH amide column. Samples were injected into the column with a volume of 1 microliter. The elution conditions were as follows: for RP, a gradient from 99% mobile phase A (0.1% formic acid in H2O) to 95% mobile phase B (0.1% formic acid in methanol) was employed for 16 minutes. For HILIC, the gradient went from 99% mobile phase A (0.1% formic acid, 10 mM ammonium acetate, 90% acetonitrile, 10% H2O) to 95% mobile phase B (0.1% formic acid, 10 mM ammonium acetate, 50% acetonitrile, 50% H2O). Both columns were operated at a temperature of 45 °C, with a flow rate of 300 microliters/minute.

Spectral data collection was carried out using a Thermo Scientific Orbitrap Exploris 480 mass spectrometer. For RP, a spray voltage of 3500 V was applied in positive mode, while for HILIC, 2500 V was used in negative mode with the H-ESI source. The ion transfer tube and vaporizer temperature were maintained at 350 °C. Compound fragmentation was achieved through data-dependent MS/MS with HCD collision energies set at 20, 40, and 80.

Metabolite processing and annotation

Data analysis was conducted using the Compound Discoverer 3.3 software by Thermo Fisher Scientific, employing an untargeted metabolomics workflow. The initial steps of the analysis involved spectral alignment and peak picking. Putative elemental compositions of unknown compounds were predicted using the exact mass, isotopic pattern, fine isotopic pattern, and MS/MS data using the built in HighChem Fragmentation Library of reference fragmentation mechanisms. Metabolite annotation was performed using an in-house database built from 1200 reference standards, spectral libraries and compound databases. First, fragmentation scans, retention time and ion mass of unknown compounds were compared with those in the in-house database. Second, fragmentation scans (MS2) searches in mzCloud were performed, which is a curated database of MSn spectra containing more than 9 million spectra and 20000 compounds. Third, predicted compositions were obtained based on mass error, matched isotopes, missing number of matched fragments, spectral similarity score (calculated by matching theoretical and measured isotope pattern), matched intensity percentage of the theoretical pattern, the relevant portion of MS, and the MS/MS scan. The mass tolerance used for estimating predicted composition

was 5 ppm. Finally, annotation was complemented by searching MS1 scans on different online databases with ChemSpider (using either the exact mass or the predicted formula). To enhance annotation coverage and add compound classes, SIRIUS, CSI:FingerID, and CANOPUS were used[117]. Compounds chemical taxonomy assignment based on chemical structure was assigned using ClassyFire[118]. Furthermore, metabolite annotation was further enhanced using CMM-RT which employs machine learning, artificial intelligence, and neural networks for more accurate predictions of Retention Times (RTs)[119]. Compounds level of annotation was assigned according to the Metabolomics Standards Initiative[120] as follows: Level 1: compounds with exact match to a standard reference compound in our in-house library, Level 2: compounds with full match to online spectral databases using mzCloud database (based on MS2 spectra matching), Level 2.1 for compounds with a full match to databases such as ChemSpider and/or CMMRT, relying on mass, molecular formula, and/or retention time, combined with annotations from SIRIUS using MS2 fragmentation patterns, Level 2.2 applied to compounds with a full match to databases (ex. ChemSpider) and CMMRT based on mass, molecular formula, and retention time, Level 2.3 encompassed compounds matching any single annotation source, Level 3.1: for matches based on molecular formulas generated through Predicted Compositions node and/or CMMRT, combined with annotations from SIRIUS using MS2 fragmentation patterns, Level 3.2 indicated matches based on molecular formulas generated through Predicted Compositions in conjunction with CMMRT. Finally, Level 3.3 represented matches based on chemical formulas from any annotation source. Following metabolite annotation, poorly annotated features were eliminated by performing manual QC on the features. QC correction was applied in Compound Discoverer using a linear regression model that retains features with a QC area RSD < 30% and was limited to a maximum correction of < 25%. Mass spectra and chromatography from duplicate annotations (for a single compound) were manually inspected for spectral quality, peak shape, and retention time following data processing with Compound Discoverer to assess if one of the multiple annotations was correct. When a single confident annotation was identified, all other duplicate feature annotations were removed. Further annotations were inspected for removal of in-source fragments.

Metaproteomics

A total of 36 samples collected in August 2018 at 10-20, 40-50 and 75-100 cm, coinciding in time and space with our metagenomic sampling were sent to the Environmental Molecular Sciences Laboratory (Richland, WA) and processed for metaproteomic analysis. In brief, proteins were extracted following lyophilization using the MPLEx extraction protocol[121] and prepared for digestion using the Filter-Aided-Sample-Preparation (FASP) method[122] demonstrated for soil[123]. Peptides were normalized to a final concentration of 0.1 μg/mL prior to injection (5 μL) to an Orbitrap Lumos Fusion Tribrid mass spectrometer (Thermo Scientific, San Jose, CA) outfitted with an in-house constructed nano-electrospray ionization interface[124]. Spray voltage was 1.8 kV with an ion transfer tube temperature of 250 °C. Fourier transform mass spectra (FT-MS) were acquired from 350-1800 *m/z* at a resolution of 60k (automatic gain control, AGC, target 4×10^5) and the top 12 FT higher-energy collisional dissociation tandem mass spectra (FT-HCD-MS/MS) were acquired in data dependent mode using an isolation window of 0.7 *m/z* (normalized collision energy of 30 and a 45 s. exclusion time) with a resolution of 50k (AGC target 1×10^5). Peptides were separated inline to the mass spectrometer using a Waters nanoACQUITY UPLC (Waters Corporation, Milford, MA). Ultra-performance liquid chromatography (UPLC) conditions have previously been described[123,125]. Measured MS/MS were searched against sample specific metagenomes (NCBI BioProject repository) to assign peptide sequences using the MS-GF+ algorithm[126] with a parameter file set to 20 ppm parent ion mass tolerance, allowing for partial tryptic peptides, and dynamic modification of oxidized methionine (+15.9949 Da). Resulting peptide data was filtered to retain peptides with a false-discovery rate less than 5% using a targeted-decoy approach[127] with adjustment of the MS-GF+ spectral probability generating function to 1.13×10^{-10}. The identified peptides were then aligned against the proteins predicted from the 697 MAGs using BLASTp v2.14.0 (-task blastp-short). Hits were filtered by best hit using BlastTab.best_hit_sorted.pl from the enveomics collection[115] and only hits with a maximum of 1 mismatch and 1 gap open were considered.

Statistical analyses

Statistical analyses were done in R version 4.2.3 (R Core Team, 2023). When testing for the impact of warming and eCO_2 on MAG relative abundance, only samples from 2016 and 2018 were used since warming was initiated in 2015, and eCO2 in 2016.

Bray-Curtis and Unifrac beta diversity were calculated from the MAG relative abundance (distance(), phyloseq)[128]. The resulting matrices were used as the response variable of a distance based redundancy analysis (dbrda(), vegan), with the full model including sampling read and depth. Stepwise model selection was used to select the best fit model (ordiR2step(), vegan). Depth specific models were created to determine if warming and eCO2 influenced community composition. This resulted in a total of four models, and temperature was calculated from the average over the month of August during the year of collection at the probe closest to the depth fraction. For the samples from the 20–30 cm depth fraction we used the temperature at 20 cm, for samples from the 40–50 cm depth fraction we used the temperature at 40 cm, for samples from the 100–125 cm depth fraction we used the temperature at 100 cm, and for samples from the 150–175 cm depth fraction we used the temperature at 200 cm.

To target specific hypotheses, we fitted multiple linear regressions for the aggregated relative abundance of MAGs in 2016 and 2018 that had the metabolic potential for pathways of interest as the response variable (lmer, lme4)[129]. Pathways of interest included homoacetogenesis via the Wood-Ljungdahl pathway, acetogenesis via fermentation, sulfate and sulfite reduction, and methylotrophic, acetoclastic, and hydrogenotrophic methanogenesis. Response variables included peat temperature and eCO_2, and we included year as a random factor, the step function (lmerTest) was used to eliminate non-significant predictors[130]. We employed Maaslin2[131] to determine multivariable association between temperature and MAG-specific abundances (min_prevalence = 0) in 2018. We did not include 2016 since year-to-year effects could not be accounted for. Fixed effects included warming only. For both hypothesis-based models and Maaslin2, each depth was processed separately, and temperature was calculated as for the distance-based redundancy analysis.

LC-MS/MS feature peak abundance values were normalized through mean normalization. Distance matrices were calculated via Bray-Curtis dissimilarity and used for permutational multivariate ANOVA (PERMANOVA) in the vegan package, with visualization in ggplot2. Log2 fold change (L2FC) values were computed for each identified feature to identify meaningful differences in compound expression across different depth. T-tests were performed to determine statistical significance between depths. The Benjamini-Hochberg procedure was used to control the false discovery rate, which provided adjusted p-values (Padj) to account for multiple testing[132]. Adjustments were made separately for RP and HILIC datasets. Compounds were then filtered based on associated Padj. values < 0.05, categorizing them as upregulated in the sample when L2FC > 0, or downregulated in the sample when L2FC < 0.

International chemical identifier keys (InChIKeys), which provide standardized, condensed text representations of chemical

compounds, were extracted. These InChIKeys were utilized to classify compounds into standard chemical taxonomy categories using ClassyFire[118]. Integration of metabolomic and metagenomic data (gene abundances) was performed with the DIABLO workflow of the R package mixOmics[133] using clr-transformed data (clr, compositions R package)[134]. For the correlation analysis, the function circosPlot was used and a minimum correlation score of 0.8 or −0.8 was set to call positively and negatively correlated variables.

Reporting summary

Further information on research design is available in the Nature Portfolio Reporting Summary linked to this article.

Data availability

The raw metagenomic sequences supporting this study are available in the NCBI BioProject repository (http://ncbi.nlm.nih.gov/bioproject) under the following accession numbers: PRJNA364951-PRJNA364992, PRJNA443580-PRJNA443616, PRJNA444884-PRJNA444890, PRJNA651484-PRJNA651504, PRJNA677007-PRJNA677020, and PRJNA697594-PRJNA697710 (see also Supplementary Data 4). Metatranscripts are also available in the NCBI BioProject repository under accession number PRJNA1257299. MAGs analyzed in this manuscript were deposited in NCBI under BioProject PRJNA1084886 (see also Supplementary Data 1). Additionally, SPRUCE Whole Ecosystems Warming (WEW) Environmental Data is available at https://doi.org/10.3334/CDIAC/spruce.032, and SPRUCE Porewater Chemistry Data for Experimental Plots is available at https://doi.org/10.3334/CDIAC/spruce.028. The mass spectrometry proteomics data were deposited in the MetaproteomeXchange Consortium via the MassIVE partner repository with accession number PXD063775 and MSV000097832. Raw mass spectrometry metabolomics (LC-MS/MS) data is available in metabolomics workbench under the Study ID ST003907 and https://doi.org/10.21228/M8KZ63. All accompanying metadata generated in this study are provided in the Supplementary Data Files. Should any raw data files be needed in another format they are available from the corresponding author upon reasonable request. Source data are provided with this paper.

References

1. Walker, A. P. et al. Biophysical drivers of seasonal variability in Sphagnum gross primary production in a northern temperate bog. *J. Geophys. Res. Biogeosci.* **122**, 1078–1097 (2017).
2. Rydin, H., Jeglum, J. K. & Bennett, K. D. *The Biology of Peatlands, 2e*. (Oxford University Press, 2013).
3. Nichols, J. E. & Peteet, D. M. Rapid expansion of northern peatlands and doubled estimate of carbon storage. *Nat. Geosci.* **12**, 917–921 (2019).
4. van Breemen, N. How Sphagnum bogs down other plants. *Trends Ecol. Evol.***10**, 270–275 (1995).
5. Bragazza, L., Parisod, J., Buttler, A. & Bardgett, R. D. Biogeochemical plant–soil microbe feedback in response to climate warming in peatlands. *Nat. Clim. Change* **3**, 273–277 (2013).
6. Shao, S. et al. Ericoid mycorrhizal fungi mediate the response of ombrotrophic peatlands to fertilization: a modeling study. *N. Phytol.***238**, 80–95 (2023).
7. IPCC. *Climate Change 2013. The Physical Science Basis. Contribution of Working Group I to the Fifth Assessment Report of the Intergovernmental Panel on Climate Change*. (Cambridge University Press, 2013).
8. Taylor, P. C. et al. Process drivers, inter-model spread, and the path forward: a review of amplified arctic warming. *Front. Earth Sci.* **9**, 758361 (2022).
9. Meredith, M. et al. Polar Regions. In: *IPCC Special Report on the Ocean and Cryosphere in a Changing Climate* (eds Pörtner, H.-O. et al.) 203–320 (Intergovernmental Panel on Climate Change, 2019).
10. Masson-Delmotte, V. et al. Contribution of working group i to the sixth assessment report of the intergovernmental panel on climate change. *Clim. Change Phys. Sci. Basis* **2**, 2391 (2021).
11. Hopple, A. et al. Massive peatland carbon banks vulnerable to rising temperatures. *Nat. Commun.* **11**, 2373 (2020).
12. Wilson, R. M. et al. Soil metaboloME RESPONSE TO WHOLE-ECOSYSTEM WARMING AT THE SPRUCE AND PEATLAND RESPONSES UNDER CHANGING ENVIRONMENTS EXPeriment. *Proc. Natl. Acad. Sci. USA* **118**, e2004192118 (2021).
13. Li, Q., Gogo, S., Leroy, F., Guimbaud, C. & Laggoun-Défarge, F. Response of peatland CO2 and CH4 fluxes to experimental warming and the carbon balance. *Front. Earth Sci.* **9**, 631368 (2021).
14. Gill, A. L., Giasson, M.-A., Yu, R. & Finzi, A. C. Deep peat warming increases surface methane and carbon dioxide emissions in a black spruce-dominated ombrotrophic bog. *Glob. Change Biol.* **23**, 5398–5411 (2017).
15. Treat, C. C. et al. Temperature and peat type control CO2 and CH4 production in Alaskan permafrost peats. *Glob. Change Biol.* **20**, 2674–2686 (2014).
16. Kirk, T. K., Connors, W. J. & Zeikus, J. G. Requirement for a growth substrate during lignin decomposition by two wood-rotting fungi. *Appl. Environ. Microbiol.* **32**, 192–194 (1976).
17. Karhu, K. et al. Temperature sensitivity of organic matter decomposition in two boreal forest soil profiles. *Soil Biol. Biochem.* **42**, 72–82 (2010).
18. Hines, M. E., Duddleston, K. N., Rooney-Varga, J. N., Fields, D. and Chanton, J. P. Uncoupling of acetate degradation from methane formation in Alaskan wetlands: connections to vegetation distribution. *Glob. Biogeochem. Cycles* **22**, 2903 (2008).
19. Duddleston, K. N., Kinney, M. A., Kiene, R. P. & Hines, M. E. Anaerobic microbial biogeochemistry in a northern bog: acetate as a dominant metabolic end product. *Glob. Biogeochem. Cycles* **16**, 11-11-11-19, (2002).
20. Drake, H. L., Horn, M. A. & Wüst, P. K. Intermediary ecosystem metabolism as a main driver of methanogenesis in acidic wetland soil. *Environ. Microbiol. Rep.* **1**, 307–318 (2009).
21. Bridgham, S. D., Cadillo-Quiroz, H., Keller, J. K. & Zhuang, Q. Methane emissions from wetlands: biogeochemical, microbial, and modeling perspectives from local to global scales. *Glob. Chang Biol.* **19**, 1325–1346 (2013).
22. Hopple, A. M. et al. Massive peatland carbon banks vulnerable to rising temperatures. *Nat. Commun.* **11**, 2373 (2020).
23. Song, T. et al. Porewater constituents inhibit microbially mediated greenhouse gas production (GHG) and regulate the response of soil organic matter decomposition to warming in anoxic peat from a Sphagnum-dominated bog. *FEMS Microbiol. Ecol.* **99**, fiad060 (2023).
24. AminiTabrizi, R. et al. Microbial sensitivity to temperature and sulfate deposition modulates greenhouse gas emissions from peat soils. *Glob. Change Biol.* **29**, 1951–1970 (2023).
25. Lozanovska, I., Kuzyakov, Y., Krohn, J., Parvin, S. & Dorodnikov, M. Effects of nitrate and sulfate on greenhouse gas emission potentials from microform-derived peats of a boreal peatland: a 13C tracer study. *Soil Biol. Biochem.* **100**, 182–191 (2016).
26. Eriksson, T., ÖQuist, M. G. & Nilsson, M. B. Production and oxidation of methane in a boreal mire after a decade of increased temperature and nitrogen and sulfur deposition. *Glob. Change Biol.* **16**, 2130–2144 (2010).
27. Bodegom, P. M. V. & Stams, A. J. M. Effects of alternative electron acceptors and temperature on methanogenesis in rice paddy soils. *Chemosphere* **39**, 167–182 (1999).

28. Wilson, D. et al. Multiyear greenhouse gas balances at a rewetted temperate peatland. *Glob. change Biol.* **22**, 4080–4095 (2016).
29. Romanowicz, E. A., Siegel, D. I., Chanton, J. P. & Glaser, P. H. Temporal variations in dissolved methane deep in the Lake Agassiz Peatlands, Minnesota. *Glob. Biogeochem. Cycles* **9**, 197–212 (1995).
30. Chasar, L., Chanton, J., Glaser, P. & Siegel, D. Methane concentration and stable isotope distribution as evidence of rhizospheric processes: comparison of a fen and bog in the Glacial Lake Agassiz Peatland complex. *Ann. Bot.* **86**, 655–663 (2000).
31. Hodgkins, S. B. et al. Soil incubations reproduce field methane dynamics in a subarctic wetland. *Biogeochemistry* **126**, 241–249 (2015).
32. Tfaily, M. M. et al. Organic matter transformation in the peat column at Marcell Experimental Forest: humification and vertical stratification. *J. Geophys. Res. Biogeosci.* **119**, 661–675 (2014).
33. Conrad, R. Contribution of hydrogen to methane production and control of hydrogen concentrations in methanogenic soils and sediments. *FEMS Microbiol. Ecol.* **28**, 193–202 (1999).
34. Wilson, R. M. et al. Hydrogenation of organic matter as a terminal electron sink sustains high CO2: CH4 production ratios during anaerobic decomposition. *Org. Geochem.* **112**, 22–32 (2017).
35. Tveit, A. T., Urich, T., Frenzel, P. & Svenning, M. M. Metabolic and trophic interactions modulate methane production by Arctic peat microbiota in response to warming. *Proc. Natl. Acad. Sci. USA* **112**, E2507–E2516 (2015).
36. ST. James, A. R., Yavitt, J. B., Zinder, S. H. & Richardson, R. E. Linking microbial Sphagnum degradation and acetate mineralization in acidic peat bogs: from global insights to a genome-centric case study. *ISME J.* **15**, 293–303 (2021).
37. Richy, E. et al. How microbial communities shape peatland carbon dynamics: new insights and implications. *Soil Biol. Biochem.* **191**, 109345 (2024).
38. Reji, L. & Zhang, X. Genome-resolved metagenomics informs the functional ecology of uncultured acidobacteria in redox oscillated sphagnum peat. *mSystems* **7**, e00055–00022 (2022).
39. Lin, X. et al. Microbial metabolic potential for carbon degradation and nutrient (nitrogen and phosphorus) acquisition in an ombrotrophic peatland. *Appl. Environ. Microbiol.* **80**, 3531–3540 (2014).
40. Lin, X., Handley, K. M., Gilbert, J. A. & Kostka, J. E. Metabolic potential of fatty acid oxidation and anaerobic respiration by abundant members of Thaumarchaeota and Thermoplasmata in deep anoxic peat. *Isme J.* **9**, 2740–2744 (2015).
41. Woodcroft, B. J. et al. Genome-centric view of carbon processing in thawing permafrost. *Nature* **560**, 49–54 (2018).
42. McCalley, C. K. et al. Methane dynamics regulated by microbial community response to permafrost thaw. *Nature* **514**, 478–481 (2014).
43. Mondav, R. et al. Discovery of a novel methanogen prevalent in thawing permafrost. *Nat. Commun.* **5**, 3212 (2014).
44. Ellenbogen, J. B. et al. Methylotrophy in the Mire: direct and indirect routes for methane production in thawing permafrost. *mSystems* **9**, e00698–00623 (2024).
45. Hanson, P. J., et al. Rapid net carbon loss from a whole-ecosystem warmed peatland. *AGU Adv.* **1**, e2020AV000163 (2020).
46. Allison, S. D. & Martiny, J. B. Resistance, resilience, and redundancy in microbial communities. *Proc. Natl Acad. Sci.* **105**, 11512–11519 (2008).
47. Cronin, D. et al. Stable states in an unstable landscape: microbial resistance at the front line of climate change. *bioRxiv* **10**, 636677 (2025).
48. Rousk, J. & Bååth, E. Growth of saprotrophic fungi and bacteria in soil. *FEMS Microbiol. Ecol.* **78**, 17–30 (2011).
49. Caro, T. A., McFarlin, J., Jech, S., Fierer, N. & Kopf, S. Hydrogen stable isotope probing of lipids demonstrates slow rates of microbial growth in soil. *Proc. Natl. Acad. Sci. USA* **120**, e2211625120 (2023).
50. LeeWays, C., McCullough, L. L., Hopple, A. M., Keller, J. K. & Bridgham, S. D. Homoacetogenesis competes with hydrogenotrophic methanogenesis for substrates in a peatland experiencing ecosystem warming. *Soil Biol. Biochem.* **172**, 108759 (2022).
51. Ofiti, N. O. E. et al. Warming and elevated CO2 promote rapid incorporation and degradation of plant-derived organic matter in an ombrotrophic peatland. *Glob. Change Biol.* **28**, 883–898 (2022).
52. Ofiti, N. O. E. et al. Climate warming and elevated CO2 alter peatland soil carbon sources and stability. *Nat. Commun.* **14**, 7533 (2023).
53. Duchesneau, K. et al. Responses of vascular plant fine roots and associated microbial communities to whole-ecosystem warming and elevated CO2 in northern peatlands. *New Phytol.* **242**, 1333–1347 (2024).
54. Hausmann, B. et al. Peatland Acidobacteria with a dissimilatory sulfur metabolism. *ISME J.* **12**, 1729–1742 (2018).
55. Dyksma, S. & Pester, M. Oxygen respiration and polysaccharide degradation by a sulfate-reducing acidobacterium. *Nat. Commun.* **14**, 6337 (2023).
56. Zhou, Z., Pan, J., Wang, F., Gu, J.-D. & Li, M. Bathyarchaeota: globally distributed metabolic generalists in anoxic environments. *FEMS Microbiol. Rev.* **42**, 639–655 (2018).
57. Liu, Y. & Whitman, W. B. Metabolic, phylogenetic, and ecological diversity of the methanogenic archaea. *Ann. N. Y. Acad. Sci.* **1125**, 171–189 (2008).
58. Megonigal, J. P., Hines, M. & Visscher, P. Anaerobic metabolism: linkages to trace gases and aerobic processes. *Biogeochemistry* **8**, 317–424 (2004).
59. Griffiths, N. A. & Sebestyen, S. D. Dynamic vertical profiles of peat porewater chemistry in a northern peatland. *Wetlands* **36**, 1119–1130 (2016).
60. Tfaily, M. M. et al. Vertical stratification of peat pore water dissolved organic matter composition in a peat bog in Northern Minnesota. *J. Geophys. Res. Biogeosci.***123**, 479–494 (2018).
61. Lin, X. et al. Microbial community stratification linked to utilization of carbohydrates and phosphorus limitation in a boreal peatland at marcell experimental forest, Minnesota, USA. *Appl. Environ. Microbiol.* **80**, 3518–3530 (2014).
62. Puglisi, E. et al. Changes in bacterial and archaeal community assemblages along an ombrotrophic peat bog profile. *Biol. Fertil. soils* **50**, 815–826 (2014).
63. Asemaninejad, A., Thorn, R. G., Branfireun, B. A. & Lindo, Z. Vertical stratification of peatland microbial communities follows a gradient of functional types across hummock–hollow microtopographies. *Écoscience* **26**, 249–258 (2019).
64. Lamit, L. J. et al. Peatland microbial community responses to plant functional group and drought are depth-dependent. *Mol. Ecol.* **30**, 5119–5136 (2021).
65. Ragsdale, S. W. & Pierce, E. Acetogenesis and the Wood–Ljungdahl pathway of CO2 fixation. *Biochimica et. Biophysica Acta Proteins Proteom.* **1784**, 1873–1898 (2008).
66. Asemaninejad, A., Thorn, R. G. & Lindo, Z. Vertical distribution of fungi in hollows and hummocks of boreal peatlands. *Fungal Ecol.* **27**, 59–68 (2017).
67. Keller, J. K. & Bridgham, S. D. Pathways of anaerobic carbon cycling across an ombrotrophic-minerotrophic peatland gradient. *Limnol. Oceanogr.* **52**, 96–107 (2007).
68. Corbett, J. E. et al. Partitioning pathways of CO 2 production in peatlands with stable carbon isotopes. *Biogeochemistry* **114**, 327–340 (2013).

69. Wilson, R. M. et al. Stability of peatland carbon to rising temperatures. *Nat. Commun.* **7**, 13723 (2016).
70. Carrell, A. A. et al. Novel metabolic interactions and environmental conditions mediate the boreal peatmoss-cyanobacteria mutualism. *ISME J.* **16**, 1074–1085 (2022).
71. Pester, M., Bittner, N., Deevong, P., Wagner, M. & Loy, A. A 'rare biosphere' microorganism contributes to sulfate reduction in a peatland. *ISME J.* **4**, 1591–1602 (2010).
72. Mesquita, C. P. B. D., Wu, D. & Tringe, S. G. Methyl-based methanogenesis: an ecological and genomic review. *Microbiol. Mol. Biol. Rev.* **87**, e00024–00022 (2023).
73. Zalman, C. A. et al. Methylotrophic methanogenesis in Sphagnum-dominated peatland soils. *Soil Biol. Biochem.* **118**, 156–160 (2018).
74. Tan, X. et al. Fe(III)-mediated anaerobic ammonium oxidation: a novel microbial nitrogen cycle pathway and potential applications. *Crit. Rev. Environ. Sci. Technol.* **52**, 2962–2994 (2022).
75. Wan, L., Liu, H. & Wang, X. Anaerobic ammonium oxidation coupled to Fe(III) reduction: discovery, mechanism and application prospects in wastewater treatment. *Sci. Total Environ.* **818**, 151687 (2022).
76. Martikainen, P. J. Heterotrophic nitrification – an eternal mystery in the nitrogen cycle. *Soil Biol. Biochem.* **168**, 108611 (2022).
77. Curtinrich, H. J., Sebestyen, S. D., Griffiths, N. A. & Hall, S. J. Warming stimulates iron-mediated carbon and nutrient cycling in mineral-poor peatlands. *Ecosystems* **25**, 44–60 (2022).
78. Petro, C. et al. Climate drivers alter nitrogen availability in surface peat and decouple N2 fixation from CH4 oxidation in the Sphagnum moss microbiome. *Glob. Change Biol.* **29**, 3159–3176 (2023).
79. Horn, M. A., Matthies, C., Küsel, K., Schramm, A. & Drake, H. L. Hydrogenotrophic methanogenesis by moderately acid-tolerant methanogens of a methane-emitting acidic peat. *Appl. Environ. Microbiol.* **69**, 74–83 (2003).
80. Conrad, R. Complexity of temperature dependence in methanogenic microbial environments. *Front. Microbiol.* **14**, 1232946 (2023).
81. Thauer, R. K., Kaster, A.-K., Seedorf, H., Buckel, W. & Hedderich, R. Methanogenic archaea: ecologically relevant differences in energy conservation. *Nat. Rev. Microbiol.* **6**, 579–591 (2008).
82. Hanson, P. J. et al. Attaining whole-ecosystem warming using air and deep-soil heating methods with an elevated CO2 atmosphere. *Biogeosciences* **14**, 861–883 (2017).
83. Hanson, P., Riggs, J., Nettles, W. R., Krassovski, M. & Hook, L. SPRUCE whole ecosystems warming (WEW) environmental data beginning August 2015. (Oak Ridge National Laboratory, 2016).
84. Griffiths, N. A. et al. SPRUCE Porewater Chemistry Data for Experimental Plots, Beginning in 2013. (ORNLTESSFA (Oak Ridge National Lab's Terrestrial Ecosystem Science, 2016).
85. Malhotra, A. et al. Peatland warming strongly increases fine-root growth. *Proc. Natl. Acad. Sci. USA* **117**, 17627–17634 (2020).
86. Iversen, C. M. et al. Whole-ecosystem warming increases plant-available nitrogen and phosphorus in an ombrotrophic bog. *Ecosystems* **26**, 86–113 (2023).
87. Sebestyen, S. D., Griffiths, N., KC, O. & Stelling, J. SPRUCE precipitation chemistry and bulk atmospheric deposition beginning in 2013. (Oak Ridge National Lab, 2020).
88. Bushnell, B., Rood, J. & Singer, E. BBMerge – accurate paired shotgun read merging via overlap. *PLoS ONE* **12**, e0185056 (2017).
89. Peng, Y., Leung, H. C. M., Yiu, S. M. & Chin, F. Y. L. IDBA-UD: a de novo assembler for single-cell and metagenomic sequencing data with highly uneven depth. *Bioinformatics* **28**, 1420–1428 (2012).
90. Bankevich, A. et al. SPAdes: a new genome assembly algorithm and its applications to single-cell sequencing. *J. Comput. Biol.* **19**, 455–477 (2012).
91. Wu, Y.-W., Simmons, B. A. & Singer, S. W. MaxBin 2.0: an automated binning algorithm to recover genomes from multiple metagenomic datasets. *Bioinformatics* **32**, 605–607 (2016).
92. Kang, D. D. et al. MetaBAT 2: an adaptive binning algorithm for robust and efficient genome reconstruction from metagenome assemblies. *PeerJ.* **7**, e7359 (2019).
93. Rodriguez-R, L. M. et al. The microbial genomes atlas (MiGA) webserver: taxonomic and gene diversity analysis of Archaea and Bacteria at the whole genome level. *Nucleic Acids Res.* **46**, W282–W288 (2018).
94. Olm, M. R., Brown, C. T., Brooks, B. & Banfield, J. F. dRep: a tool for fast and accurate genomic comparisons that enables improved genome recovery from metagenomes through de-replication. *ISME J.* **11**, 2864–2868 (2017).
95. Parks, D. H., Imelfort, M., Skennerton, C. T., Hugenholtz, P. & Tyson, G. W. CheckM: assessing the quality of microbial genomes recovered from isolates, single cells, and metagenomes. *Genome Res.* **25**, 1043–1055 (2015).
96. Parks, D. H. et al. A complete domain-to-species taxonomy for Bacteria and Archaea. *Nat. Biotechnol.* **38**, 1079–1086 (2020).
97. Shaffer, M. et al. DRAM for distilling microbial metabolism to automate the curation of microbiome function. *Nucleic acids Res.* **48**, 8883–8900 (2020).
98. Aroney, S. T. N. et al. CoverM: read alignment statistics for metagenomics. *Bioinformatics* **41**, btaf147 (2025).
99. Nayfach, S. & Pollard, K. S. Average genome size estimation improves comparative metagenomics and sheds light on the functional ecology of the human microbiome. *Genome Biol.* **16**, 51 (2015).
100. Hyatt, D. et al. Prodigal: prokaryotic gene recognition and translation initiation site identification. *BMC Bioinforma.* **11**, 119 (2010).
101. Asnicar, F. et al. Precise phylogenetic analysis of microbial isolates and genomes from metagenomes using PhyloPhlAn 3.0. *Nat. Commun.* **11**, 2500 (2020).
102. Yu, G., Smith, D. K., Zhu, H., Guan, Y. & Lam, T. T.-Y. ggtree: an r package for visualization and annotation of phylogenetic trees with their covariates and other associated data. *Methods Ecol. Evol.* **8**, 28–36 (2017).
103. Kopylova, E., Noé, L. & Touzet, H. SortMeRNA: fast and accurate filtering of ribosomal RNAs in metatranscriptomic data. *Bioinformatics* **28**, 3211–3217 (2012).
104. Johnston, E. R. et al. Phosphate addition increases tropical forest soil respiration primarily by deconstraining microbial population growth. *Soil Biol. Biochem.* **130**, 43–54 (2019).
105. Ondov, B. D. et al. Mash: fast genome and metagenome distance estimation using MinHash. *Genome Biol.* **17**, 132 (2016).
106. Dixon, P. VEGAN, A Package of R Functions for Community Ecology. *J. Vege. Sci.* **14**, 927–930 (2003).
107. Valero-Mora, P. M. ggplot2: Elegant Graphics for Data Analysis. *J. Stat. Softw. Book Rev.* **35**, 1–3 (2010).
108. Jain, C., Rodriguez-R, L. M., Phillippy, A. M., Konstantinidis, K. T. & Aluru, S. High throughput ANI analysis of 90K prokaryotic genomes reveals clear species boundaries. *Nat. Commun.* **9**, 5114 (2018).
109. Roco, C. A. et al. Using metagenomics to reveal landscape scale patterns of denitrifiers in a montane forest ecosystem. *Soil Biol. Biochem.* **138**, 107585 (2019).
110. Liu, H.-N., Hsu, T.-W., Wu, Y.-H. & Huang, C.-L. Unraveling microbiomes associated with decomposition of needles of two Pinus species with contrasting fire-adaptive strategies. *Biol. Fertil. Soils* **57**, 715–729 (2021).

111. Luo, C. et al. Soil microbial community responses to a decade of warming as revealed by comparative metagenomics. *Appl. Environ. Microbiol.* **80**, 1777–1786 (2014).
112. Orellana, L. H., Chee-Sanford, J. C., Sanford, R. A., Löffler, F. E. & Konstantinidis, K. T. Year-round shotgun metagenomes reveal stable microbial communities in agricultural soils and novel ammonia oxidizers responding to fertilization. *Appl. Environ. Microbiol.* **84**, e01646–01617 (2018).
113. Sievert, C. *Interactive web-based data visualization with R, plotly, and shiny*. (CRC Press, 2020).
114. Steinegger, M. & Söding, J. Clustering huge protein sequence sets in linear time. *Nat. Commun.* **9**, 2542 (2018).
115. Rodriguez-R, L. M. & Konstantinidis, K. T. The enveomics collection: a toolbox for specialized analyses of microbial genomes and metagenomes. Report No. 2167-9843, (PeerJ Preprints, 2016).
116. Aramaki, T. et al. KofamKOALA: KEGG Ortholog assignment based on profile HMM and adaptive score threshold. *Bioinformatics* **36**, 2251–2252 (2019).
117. Dührkop, K. et al. SIRIUS 4: a rapid tool for turning tandem mass spectra into metabolite structure information. *Nat. Methods* **16**, 299–302 (2019).
118. Djoumbou Feunang, Y. et al. ClassyFire: automated chemical classification with a comprehensive, computable taxonomy. *J. Cheminf.* **8**, 61 (2016).
119. García, C. A., Gil-de-la-Fuente, A., Barbas, C. & Otero, A. Probabilistic metabolite annotation using retention time prediction and meta-learned projections. *J. Cheminf.* **14**, 33 (2022).
120. Sumner, L. W. et al. Proposed minimum reporting standards for chemical analysis. *Metabolomics* **3**, 211–221 (2007).
121. Nakayasu, E. rnesto, et al. MPLEx: a robust and universal protocol for single-sample integrative proteomic, metabolomic, and lipidomic analyses. *mSystems* **1**, 00043–00016 (2016).
122. Wiśniewski, J. R., Zougman, A., Nagaraj, N. & Mann, M. Universal sample preparation method for proteome analysis. *Nat. Methods* **6**, 359–362 (2009).
123. Callister, S. J. et al. Addressing the challenge of soil metaproteome complexity by improving metaproteome depth of coverage through two-dimensional liquid chromatography. *Soil Biol. Biochem.* **125**, 290–299 (2018).
124. Kelly, R. T. et al. Chemically Etched Open Tubular and Monolithic Emitters for Nanoelectrospray Ionization Mass Spectrometry. *Anal. Chem.* **78**, 7796–7801 (2006).
125. Zhu, Y. et al. Subnanogram proteomics: Impact of LC column selection, MS instrumentation and data analysis strategy on proteome coverage for trace samples. *Int. J. Mass Spectrom.* **427**, 4–10 (2018).
126. Kim, S., Gupta, N. & Pevzner, P. A. Spectral probabilities and generating functions of tandem mass spectra: a strike against decoy databases. *J. Proteome Res.* **7**, 3354–3363 (2008).
127. Elias, J. E. & Gygi, S. P. Target-decoy search strategy for increased confidence in large-scale protein identifications by mass spectrometry. *Nat. Methods* **4**, 207–214 (2007).
128. McMurdie, P. J. & Holmes, S. phyloseq: an R package for reproducible interactive analysis and graphics of microbiome census data. *PloS one* **8**, e61217 (2013).
129. De Boeck, P. et al. The estimation of item response models with the lmer function from the lme4 package in R. *J. Stat. Softw.* **39**, 1–28 (2011).
130. Kuznetsova, A., Brockhoff, P. B. & Christensen, R. H. B. lmerTest package: tests in linear mixed effects models. *J. Statist. Softw.* **82**, 1–26 (2017).
131. Mallick, H. et al. Multivariable association discovery in population-scale meta-omics studies. *PLoS Comput. Biol.* **17**, e1009442 (2021).
132. Benjamini, Y. & Hochberg, Y. Controlling the false discovery rate: a practical and powerful approach to multiple testing. *J. R. Stat. Soc. Ser. B* **57**, 289–300 (1995).
133. Singh, A. et al. DIABLO: an integrative approach for identifying key molecular drivers from multi-omics assays. *Bioinformatics* **35**, 3055–3062 (2019).
134. van den Boogaart, K. G. & Tolosana-Delgado, R. compositions": a unified R package to analyze compositional data. *Comp. Geosci.* **34**, 320–338 (2008).

Acknowledgements

We are thankful to the editor and reviewers for their attentive and considerate comments. This study was funded by the Office of Biological and Environmental Research, Terrestrial Ecosystem Science Program and Genomic Science programs, under US Department of Energy (DOE) Contract DE-SC0023297 (JEK). The work (proposal: 10.46936/10.25585/60001027) conducted by the U.S. Department of Energy Joint Genome Institute (https://ror.org/04xm1d337), a DOE Office of Science User Facility, is supported by the Office of Science of the U.S. Department of Energy operated under Contract No. DE-AC02-05CH11231. A portion of this research was performed on a project award (https://doi.org/10.46936/sthm.proj.2016.49279/60005943) from the Environmental Molecular Sciences Laboratory, a DOE Office of Science User Facility sponsored by the Biological and Environmental Research program under Contract No. DE-AC05-76RL01830. The SPRUCE experiment is funded by the Biological and Environmental Research program in the U.S. Department of Energy's Office of Science. We also acknowledge the important SPRUCE onsite contributions made by W. Robert Nettles and Jeff Riggs who managed and sustained the SPRUCE experimental and warming treatments, and environmental monitoring systems. We would also like to acknowledge Karl K. Weitz from the Biological Sciences Division at PNNL for running the proteomic samples on the mass spectrometer.

Author contributions

Experimental design: C.W.S., J.E.K., K.T.K., and P.J.H. Environmental monitoring: P.J.H. Field sampling: C.P., M.G., K.D., C.W.S., S.W.R., and E.R.J. Pore water chemistry: R.W. and J.P.C. Metabolite data: M.T. and G.M. Metaproteomics data: J.B.T., S.J.C., and S.O.M. Microbial data: K.D., S.W.R., E.R.J., L.A.K., S.T., E.E.F., and T.G.D.R. Data analysis: B.A.R. and K.D. Writing: B.A.R. and K.D. All authors commented on and edited the manuscript.

Competing interests

The authors declare no competing interests.

Additional information

Supplementary information The online version contains supplementary material available at https://doi.org/10.1038/s41467-025-61664-7.

Correspondence and requests for materials should be addressed to Joel E. Kostka.

Peer review information *Nature Communications* thanks Sanjay Swarup, and the other, anonymous, reviewers for their contribution to the peer review of this work. A peer review file is available.

[1]School of Biological Sciences and School of Earth and Atmospheric Sciences, Center for Microbial Dynamics and Infection, Georgia Institute of Technology, Atlanta, GA, USA. [2]School of Civil & Environmental Engineering and School of Biological Sciences, Georgia Institute of Technology, Atlanta, GA, USA. [3]Department of Environmental Science, University of Arizona, Tucson, AZ, USA. [4]Department of Earth, Ocean and Atmospheric Science, Florida State University, Tallahassee, FL, USA. [5]Biosciences Division, Oak Ridge National Laboratory, Oak Ridge, TN, USA. [6]Environmental Sciences Division, Oak Ridge National Laboratory, Oak Ridge, TN, USA. [7]Biological Sciences Division, Pacific Northwest National Laboratory, US Department of Energy, Richland, WA, USA. [8]Environmental Molecular Sciences Laboratory, Pacific Northwest National Laboratory, US Department of Energy, Richland, WA, USA. [9]DOE Joint Genome Institute, Lawrence Berkeley National Laboratory, Berkeley, CA, USA. [10]These authors contributed equally: Katherine Duchesneau, Borja Aldeguer-Riquelme. ✉e-mail: joel.kostka@biology.gatech.edu